HHS Public Access

Author manuscript

Dev Biol. Author manuscript; available in PMC 2020 June 15.

Published in final edited form as:

Dev Biol. 2019 June 15; 450(2): 101–114. doi:10.1016/j.ydbio.2019.03.018.

Trim33 is required for appropriate development of pre-cardiogenic mesoderm

Sudha Rajderkar[a,1], **Jeffrey M. Mann**[a], **Christopher Panaretos**[a], **Kenji Yumoto**[a], **Hong-Dong Li**[b], **Yuji Mishina**[a], **Benjamin Ralston**[a], and **Vesa Kaartinen**[a,*]

[a]Department of Biologic and Materials Sciences, University of Michigan, Ann Arbor, MI, 48109, USA

[b]Center for Bioinformatics, School of Information Science and Engineering, Central South University, Changsha, Hunan, 410083, PR China

Abstract

Congenital cardiac malformations are among the most common birth defects in humans. Here we show that Trim33, a member of the Tif1 subfamily of tripartite domain containing transcriptional cofactors, is required for appropriate differentiation of the pre-cardiogenic mesoderm during a narrow time window in late gastrulation. While mesoderm-specific *Trim33* mutants did not display noticeable phenotypes, epiblast-specific *Trim33* mutant embryos developed ventricular septal defects, showed sparse trabeculation and abnormally thin compact myocardium, and died as a result of cardiac failure during late gestation. Differentiating embryoid bodies deficient in *Trim33* showed an enrichment of gene sets associated with cardiac differentiation and contractility, while the total number of cardiac precursor cells was reduced. Concordantly, cardiac progenitor cell proliferation was reduced in *Trim33*-deficient embryos. ChIP-Seq performed using antibodies against Trim33 in differentiating embryoid bodies revealed more than 4000 peaks, which were significantly enriched close to genes implicated in stem cell maintenance and mesoderm development. Nearly half of the Trim33 peaks overlapped with binding sites of the Ctcf insulator protein. Our results suggest that Trim33 is required for appropriate differentiation of precardiogenic mesoderm during late gastrulation and that it will likely mediate some of its functions via multi-protein complexes, many of which include the chromatin architectural and insulator protein Ctcf.

*Corresponding author. vesak@umich.edu (V. Kaartinen).

[1]Current address: Environmental Genomics and Systems Biology Division, Lawrence Berkeley National Laboratory, Berkeley, CA 94720, USA.

The data availability statement

The RNA-Seq and ChIP-Seq data discussed in this manuscript have been deposited in NCBI's Gene expression Omnibus and are accessible through GEO Series accession numbers GSE80166 (https://www.ncbi.nlm.nih.gov/geo/query/acc.cgi?acc=GSE80166) and GSE119874 (https://www.ncbi.nlm.nih.gov/geo/query/acc.cgi?acc=GSE119874).

Appendix A. Supplementary data

Supplementary data to this article can be found online at https://doi.org/10.1016/j.ydbio.2019.03.018.

1. Introduction

Ventricular septal defects (VSDs) are the most common cardiac defect in childhood (Minette and Sahn, 2006). They can be generally classified as membranous or muscular VSDs depending on the location of the defect. Membranous VSDs are caused by inadequate development or misalignment of atrio-ventricular cushions, or inappropriate elongation or alignment of outflow tract cushions, while muscular VSDs are caused by disturbed alignment of myofibers or insufficient coalescence of trabeculae (Gittenberger-de Groot et al., 2014). Studies using different model systems have shown that many cell types, e.g., neural crest, endocardial, myocardial and epicardial cells, as well as all morphogenetic signaling processes contribute to ventricular septum development (Niessen and Karsan, 2008; Poelmann et al., 2016; Rao and Harris, 2018). However, precise molecular control of such complicated cellular and molecular processes is currently not well known. Here we have investigated the regulatory role of Trim33, a poorly characterized transcriptional co-factor in early cardiac development and its implications to myocardial differentiation and ventricular septum formation.

Trim33 belongs to the Tif1 subfamily of tripartite domain containing proteins. In addition to the N-terminal tripartite domain (composed of a RING finger domain, two B-box zinc finger domains and coiled coil region), Trim33 contains a Smad binding region, and a tandem of PHD and Bromo domains at its C-terminal end (Venturini et al., 1999). These structural characteristics imply that Trim33 possesses both E3 ubiquitin ligase and chromatin binding activities. Subsequent studies have shown that the effect of Trim33 on cellular function is plastic and highly context dependent. In erythroid cells, Trim33 has been shown to function as an elongation factor, while in epithelial and malignant cell lines, Trim33 was shown to repress TGF-β signaling by monoubiquitinating Smad4 via a mechanism that involves Trim33-histone interactions (Agricola et al., 2011; Dupont et al., 2009). An opposite role for Trim33 in regulation of TGF-β signaling was suggested in mesendoderm induction (Xi et al., 2011). In this context, Trim33 was shown to promote TGF-β signaling by functioning as a chromatin reader, which regulates access of R-Smad:Smad4 transcriptional complexes to their *bona fide* response elements (Xi et al., 2011). A common theme in Trim33-regulated biological events seems to be that its functions are limited to situations where differentiation of progenitor cell populations is required (Rajderkar et al., 2017); thus Trim33 has little or no relevance in homeostatic cellular responses. Concordantly, tissue-specific *Trim33* mutants show defects in neural stem cell differentiation (Falk et al., 2014), in hematopoiesis (Quere et al., 2014; Tanaka et al., 2018; Wang et al., 2015), in malignant transformation (Aucagne et al., 2011; Pommier et al., 2015; Vincent et al., 2012) and in other physiological conditions where cellular plasticity is required and/or intense tissue remodeling takes place, such as terminal differentiation of mammary epithelium and lactation (Hesling et al., 2013).

A previous study showed that mouse embryos lacking *Trim33* (global knockouts) die at gastrulation before E7.5 with severe defects in tissue patterning and embryonic polarity (Morsut et al., 2010). These phenotypes significantly differ from those described in two other studies (Isbel et al., 2015; Kim and Kaartinen, 2008), which showed that global *Trim33* knockout embryos undergo neurulation and die around E9.5 suggesting that *Trim33* is not required for gastrulation *in vivo*. To clarify the developmental role of Trim33 in the

embryo proper during mesendoderm induction, we deleted *Trim33* specifically in the epiblast using the *Sox2Cre* driver line. Our results show that epiblast-specific ablation of *Trim33* does not result in early embryonic death during or soon after gastrulation. Instead, *Trim33:Sox2Cre* mutants develop ventricular septal, trabecular and myocardial defects, while deletion of *Trim33* in the mesendoderm, cardiogenic mesoderm or in neural crest does not result in major developmental phenotypes. Our results imply that Trim33 regulates precardiogenic mesoderm development, and that its absence leads to an aberrant cardiogenic differentiation ultimately resulting in myocardial and ventricular septal defects during late gestation.

2. Experimental Procedures

2.1. Ethics statement

This research was conducted in strict accordance with the recommendations in the Guide for the Care and Use of Laboratory Animals of the National Institutes of Health. The experiments described here are specifically approved by the Institutional Animal Care and Use Committee at the University of Michigan-Ann Arbor (Protocol Number: PRO00007157).

2.2. Mice

$Trim33^{FF}$, *Nkx2-5Cre, Mox2Cre, Sox2Cre, Tie2Cre, Wnt1Cre, TCre and $UbcCre^{ERT2}$* and *$Smad4^{FF}$* have been described earlier (Danielian et al., 1998; Kim and Kaartinen, 2008; Koni et al., 2001; Moses et al., 2001; Perantoni et al., 2005; Tallquist and Soriano, 2000; Yang et al., 2002). Timed matings between $Trim33^{KO/WT}$ and appropriate Cre^{+} male and $Trim33^{FF}$ or $Trim33^{FWT}$ female mice were used to obtain $Trim33^{FKO}:Cre^{+}$ tissue-specific mutant embryos. Controls were either $Trim33^{FWT}:Cre^{-}$ or on occasion $Trim33^{FWT}:Cre^{+}$ when explicitly indicated. All animals used in this study were in a mixed genetic background.

2.3. Establishment of embryonic stem cell lines and EB culture

Mouse ES cells were derived from $Trim33^{FF}:UbcCre^{ERT2}$ blastocysts as described in (Pieters et al., 2012). ESCs were passaged in serum-containing medium (Life Technologies, Cat. No. 16141–061), dissociating with TrypLE Express (Life Technologies, Cat. No. 12605–010) and maintained in serum replacement medium (Knock Out Serum Replacement Cat. No. 10828–010, Life Technologies) in a base medium of 1:1 Knock Out Dulbecco's Modified Eagle's Medium and Ham's F12. $Trim33^{FF}:UbcCre^{ERT2}$ ESCs were maintained under feeder-free culture conditions on gelatin-coated dishes in the presence of 2i (1.0 μM PD0325901 and 3 μM CHIR99021; Stemgent) and LIF (Millipore; ESG 1106). EB formation and differentiation were carried out per the ATCC protocol in 20% serum containing medium (http://diyhpl.us/~bryan/irc/protocol-online/protocol-cache/Embryoid_Body_Formation.pdf). Both the media for non-differentiating and differentiating conditions were supplemented by Glutamine (GlutaMAX-l, Life Technologies, Cat. No. 35050–061), β-mercaptoethanol (Life Technologies, Cat. No. 21985–023) and Penicillin/Streptomycin (Life Technologies, Cat. No.15140–122). 4-hydroxytamoxifen (4-OHT) (Sigma, Cat. No. T176) was added at intended and precise time points in a concentration of 1 μg/ml. Percentage of contracting EBs were counted and averaged in 3 independent sample

pairs, in 6 separate areas of each culture dish, at the same time point on days 9, 10 and 11 in a genotype-blind manner by 2 independent observers.

For relevant experiments, control and Trim33 mutant EBs were treated with 100 ng/ml of rh/m/rActivin A (R&D Systems, Cat. No. A338-AC) for 40 min.

2.4. Histology

Mouse embryos were harvested in sterile DPBS and fixed overnight in commercial 10% formalin or freshly made 4% paraformaldehyde in PBS at 4 °C overnight. Samples for histology as well as immunohistochemistry were processed in a standard paraffin-embedding protocol. Briefly, embryonic tissues were washed, dehydrated, oriented in the desired plane and embedded in fresh Blue Ribbon Tissue Embedding/Infiltration Medium (Leica Surgipath). 7 μm serial sections were mounted on Superfrost plus slides (Fisher) and stored at either room temperature or 4 °C. Hematoxylin and eosin staining was performed using a standard protocol.

Thickness of the compact myocardium was measured by using the Olympus DP73 software package. Five independent sample pairs in 6 separate areas per sample in serial sections were used. The thickness measurement was correlated with the number of cell layers present by counting nuclei across the thickness of the wall; control measurements were consistent with previously described data (Sedmera et al., 2000).

The extent of trabeculation was measured on histological sections by analyzing the area the trabeculae covered in ventricles by using ImageJ. The results were presented as percentage of surface area covered by trabecular tissue over total area of the standard size field. The fields were chosen adjacent to the compact myocardium. At minimum, 4 sections per sample were analyzed (n = 3 for each genotype).

DAPI-dilactate stainings were performed according to protocol of Sandell et al. (2012). Stained embryos were photographed using the Leica M165FC epifluorescence stereomicroscope with DP73 and software.

2.5. RNA-Seq

Equivalent amounts/number of EBs were collected at Day 7 in duplicate mutant-control pairs (4-OHT induction at day 4) in 100–200 μl of commercially available (Qiagen) RLT buffer. Total RNAs were isolated by using the Qiagen RNesy Mini Kit (Cat. No. 74104). Sequencing libraries were prepared by the University of Michigan DNA Sequencing Core and reads were generated on Illumina HiSeq2000. After quality assessment per sample, single-end, 52 base pair reads were aligned to mm9 (mus musculus assembly July 2007) by using the STAR RNA Seq aligner (Dobin et al., 2013). Read counts for differential expression were obtained using HTSeq program. Differential expression analyses were performed by using the DESeq program in the R Statistical Package https://bioconductor.org/packages/3.3/bioc/vignettes/DESeq/inst/doc/DESeq.pdf.

2.6. Immunohistochemistry

Embryos were rinsed in PBS, fixed overnight in 4% buffered paraformaldehyde at 4 °C;, washed, processed through sucrose gradient to OCT compound and embedded for frozen sectioning. 10 μm sections were stained with primary antibodies overnight at 4 °C. Binding was visualized with Alexafluor-594 or −488-conjugated secondary antibodies (Life Technologies) on slides mounted with Vectashield/DAPI (Vector Labs). For EdU assay, 100 μl of EdU labeling reagent (1 mg/ml) was injected IP, tissues were harvested 1 h later, and processed for sectioning. Sections were stained using the Click-iT EdU Alexa Fluor 488 Imaging Kit (Molecular Probes C10337). Hypoxic regions on palatal tissues were analyzed using the Hypoxyprobe kit (Hypoxyprobe Inc HPI-100) according to manufacturer's instructions.

2.7. Transfection, immunoprecipitation and western blot assays

EBs at day 6 of differentiation were dissociated with Trypsin, plated and transfected with full-length Myc/Flag-tagged mTrim33 cDNA (Origene MR227454) and full-length mCtcf cDNA (Origene MC202667) using ViaFect Transfection reagent (Promega PRE4981). After 48 h, cells, embryoid bodies were lysed in Pierce IP-lysis buffer (Thermoscientific, Prod. #87787) supplemented with Roche proteinase inhibitor cocktail (11836153001), sodium fluoride (NaF) and sodium orthovanadate (Na_3VO_4) to a final concentration of 1 mM. The cleared lysates were immunoprecipitated using a monoclonal anti-Flag antibody. The washed precipitates were analyzed using Western blotting. Briefly, the protein lysates were denatured in 2 × Laemmli lysis buffer under reducing conditions, proteins were resolved on NuPAGE BisTris SDS-PAGE gels (Invitrogen) using the X-Cell SureLock Mini-Cell electrophoresis system (Thermo-Fisher) according to the manufacturer's instructions. After electrotransfer to nitrocellulose membrane (iBlot, Thermo-Fisher), the filters were blocked (5% milk in TBST) and probed with specific antibodies, followed by HRP-conjugated secondary antibodies. Immunoblots were visualized using ECL reagents (Pierce) and BioSpectrum AC imaging system (UVP). The band intensities were analyzed using BioSpectrum.

AC imaging system. The antibodies used have been summarized in Table 1.

2.8. In situ hybridization

DIG-labeled RNA probes were made using a DIG-labeled NTP mix (Roche Applied Sciences) according to manufacturer's instructions and stored at −80 °C or at −20 °C when diluted in the hybridization buffer (for details see Table 2). Embryos for whole mount ISH were fixed in freshly thawed 4% paraformaldehyde in PBS overnight, washed in PBST, dehydrated and stored in 95% methanol, 5% PBST at −20 °C. After rehydration, the samples were treated with Proteinase K (Invitrogen, Cat.No. 25530-049 in final concentration of 10 μg/ml), post-fixed and prehybridized rotating for at least 1 h in standard non-SDS-based hybridization buffer, pH 5, at 70 °C. The probes were added in a final concentration of 0.1–1 ng/μl and left rolling overnight (o/n). Embryos were subsequently washed in a roller set-up for 20 min three times in preheated hybridization buffer at 70 °C, once in hybridization buffer/TBST, then in at least 6 changes TBST at room temperature (RT) over 1 h, blocked in 2% Roche block (one hour) and rocked o/n at 4 °C with α-DIG Fab fragments (Roche

Applied Sciences, 1:2000–5000). Samples were thoroughly washed with several changes of TBST the next day at room temperature and then o/n at 4 °C. On Day 4, samples were equilibrated for 10 min (RT) twice in NTMT pH 9.5 in a roller set up, and stained with BM Purple AP (Roche Applied Sciences) substrate at RT in the dark for several hours. Stained embryos were washed thoroughly in PBS, fixed in 4% paraformaldehyde and stored at 4 °C. Stained embryos were imaged immediately and processed for routine genotyping post-staining, postfixing upon satisfactory documentation of ISH results.

2.9. Echocardiography

At day 11.5 dpc, pregnant *Trim33*^{FF}female mice crossed with *Trim33*^{FKO}*:Sox2Cre*$^{+}$ male mice were induced with anesthesia in an enclosed container filled with 4% isoflurane. After induction, the mice were placed on a warming pad to maintain body temperature. 1–1.5% isoflurane was supplied via nose cone to maintain a surgical plane of anesthesia. The hair was removed from the upper abdominal and thoracic area with depilatory cream. Both uterine horns were surgically accessed and embryos were monitored for ECG with non-invasive resting ECG electrodes. Two-dimensional, M-mode, Doppler and tissue Doppler echocardiographic images were recorded using a Visual.

Sonics' Vevo 770 high resolution *ex vivo* micro-imaging system for each embryo in a genotype-blind manner. Data from each embryo recording were systematically indexed and genotyping material was collected to correlate with findings after the actual experiment. Data were recorded for the following parameters: heart rate (HR) beats per minute (BPM), velocity mm per second for both dorsal aorta (DA) and umbilical artery (UA), Velocity Time Interval (VTI) in mm for DA and UA, Ejection Time (ET) in msec measured in the DA.

2.10. FACS assays

Day 6 EBs were dissociated with trypsin. Embryonic livers harvested at E13 were mechanically dissociated by pushing the tissues through a 70 μm cell strainer. Cells were immunostained at 4 °C in PBS/0.5% BSA in the presence of fluoroprobe-conjugated antibodies (for details, see Table 1). The cells were washed and analyzed on flow cytometer BD FACSAria II from BD Biosciences.

2.11. ChIP-Seq

Embryoid bodies from 20 10-cm dishes were harvested at day 6 and fixed immediately with 1% p-formaldehyde for 15 min at room temperature and quenched with 0.125 M glycine. ChIP and Illumina sequencing and data analyses were carried out in Active Motif Inc (Carlsbad, CA). Briefly, chromatin was isolated by the addition of lysis buffer, followed by disruption with a Dounce homogenizer. Lysates were sonicated and the DNA sheared to an average length of 300–500 bp. Genomic DNA (Input) was prepared by treating aliquots of chromatin with RNase, proteinase K and heat for de-crosslinking, followed by ethanol precipitation. Pellets were resuspended and the resulting DNA was quantified on a NanoDrop spectrophotometer. Extrapolation to the original chromatin volume allowed quantitation of the total chromatin yield.

An aliquot of chromatin (30 μg) was precleared with protein A agarose beads (Invitrogen). Genomic DNA regions of interest were isolated using 4 μg of antibody against Trim33 (Bethyl A301–060A), Ctcf (Active Motif 61311) and H3K27ac (Active Motif 39133) (Table 1).Complexes were washed, eluted from the beads with SDS buffer, and subjected to RNase and proteinase K treatment. Crosslinks were reversed by incubation overnight at 65 °C, and ChIP DNA was purified by phenolchloroform extraction and ethanol precipitation.

Illumina sequencing libraries were prepared from the ChIP and Input DNAs by the standard consecutive enzymatic steps of end-polishing, dAaddition, and adaptor ligation. After a final PCR amplification step, the resulting DNA libraries were quantified and sequenced on Illumina's NextSeq 500 (75 nt reads, single end). Reads were aligned to the mouse genome (mm10) using the BWA algorithm (default settings). Duplicate reads were removed and only uniquely mapped reads (mapping quality ≥25) were used for further analysis. Alignments were extended in silico at their 3'-ends to a length of 200 bp, which is the average genomic fragment length in the size-selected library, and assigned to 32-nt bins along the genome. The resulting histograms (genomic "signal maps") were stored in bigWig files. Trim33, Ctcf and H3K27Ac peak locations were determined using the MACS algorithm (v2.1.0) with a cutoff of p-value = 1e-7 (Zhang et al., 2008). Peaks that were on the ENCODE blacklist of known false ChIP-Seq peaks were removed. Signal maps and peak locations were used as input data to Active Motifs proprietary analysis program, which creates Excel tables containing detailed information on sample comparison, peak metrics, peak locations and gene annotations.

2.12. ChIP-qPCR

Control and mutant EBs were fixed cross-linked with 1% formaldehyde for 30 min, washed and sonicated on ice for 8 min (1s on - 1s off sonication cycle; 50% power output) using the Sonic Ruptor 250 sonicator equipped with a microtip (Omni International). Chromatin immunoprecipitation using ChIP-qualified anti-Trim33 antibody (Bethyl A301– 060A) was carried out using the SimpleChIP Plus Sonication ChIP kit (#56383 Cell Signaling Technology) following the manufacturer's instructions. qPCR reactions were carried out using the Applied Biosystems ViiA7 real-time PCR system and Power SYBR Green PCR master mix (Thermo Fisher 4367659). Primer sequences used in PCR reactions are shown in Table 3. Binding efficiency was calculated using percentage of IP'ed chromatin against input chromatin.

2.13. Statistical analyses

Three or more independent samples were analyzed in each assay (details given in Figure texts). Averages, standard error and probability (unpaired two-tailed Student's t-test) were calculated and p-values of less than 0.05 were marked as significant.

3. Results

3.1. Trim33 is expressed in mouse embryos before, during and after mesendoderm induction

To gain a deeper understanding of the role of Trim33 in mouse embryos during and after mesoderm induction, we first assessed stage-specific Trim33 expression in early mouse embryos using a specific anti-Trim33 antibody in immunohistochemistry assays. We show that Trim33 protein is abundantly expressed in pre-streak stage embryos. Particularly, all epiblast cells display strong nuclear staining, while cells in the visceral endoderm show scattered weak staining (Fig. 1A). In mid-streak stage embryos, nuclear staining can be seen both in cells under-going mesoderm induction (double positive for both Brachyury (T, mesoderm marker) and for Trim33), and in T-negative ectoderm cells (Fig. 1B). In the head-fold stage embryos, all ectoderm and mesoderm cells show strong nuclear staining, while the endoderm is mostly negative for Trim33 (Fig. 1C). In addition, many extra-embryonic tissues, e.g., chorion, allantois and amniotic ectoderm show positively staining nuclei (Fig. 1C).

3.2. Trim33 is required in the cardiogenic mesoderm for normal cardiac development during a narrow time window close to late gastrulation

Two previous studies have suggested a critical function for *Trim33* in mesendoderm formation (Morsut et al., 2010; Xi et al., 2011), while our previous report (Kim and Kaartinen, 2008) and the study of Isbel et al. (2015) concluded that Trim33 is not required for this process. To clarify the role of Trim33 in mesendoderm induction and early lineage specification, we generated epiblast-specific and mesendoderm-specific knockouts by using the driver lines shown in Table 4. Detailed histological analyses of epiblast-specific *Trim33:Sox2Cre* mutants did not show obvious morphological defects at E11.5 and they were obtained nearly at the expected Mendelian frequency (60/278 vs. 73/278) (Fig. 2B). At later stages starting at E13, we obtained fewer than expected mutant embryos with very few surviving through E15 (Fig. 2B). No viable $Trim33^{FF}$*:Sox2Cre* embryos were obtained at birth. Cardiac edema (n = 10) was frequently detected among the mutant embryos collected at E13.5 (n = 31; Fig. 2C).

Gestational lethality in mouse embryos at E10-E13 has been attributed to two most likely causes: defects in cardiac/circulatory function and/or a hematopoietic deficiency (Papaioannou and Behringer, 2012). Previous studies have shown that Trim33 promotes erythroid differentiation (He et al., 2006) and regulates transcriptional elongation of erythroid genes (Bai et al., 2010, 2013). Thus we quantified premature and mature erythroblasts in controls and $Trim33^{FF}$*:Sox2Cre* mutants at E13.5 by FACS (Koulnis et al., 2011). A modest reduction detected in both $CD71^{HI}Ter119^{HI}$ (proerythroblasts) and $Ter119^{HI}CD71^{LO}$ (erythroblasts) cell populations was too subtle to result in embryonic death (Supplemental Fig. 1A). Immunostaining for CD31 (endothelial marker) did not reveal any gross differences between controls and mutants suggesting that, by and large, vasculature was not significantly affected (Supplemental Fig. 1B). Next, we compared cardiac function between control and $Trim33^{FF}$*:Sox2Cre* mutants at E11.5 using echocardiography. This assay identified 2 out of 4 $Trim33^{FF}$*:Sox2Cre* mutants that displayed

arrhythmia and cardiac failure (Supplemental Fig. 1C), which, together with our finding of cardiac edema (Fig. 1C) often associated with cardiac failure, led us to investigate the cardiac phenotype of developing *Trim33*^{FF}*:Sox2Cre* mutants in detail.

Serial sections of cardiac tissues across all the examined *Trim33*^{FF}*:Sox2Cre* mutants showed VSDs, sparse trabeculae and thinning of the ventricular myocardium (Fig. 2D, D', E, E', 2G and Supplemental Fig. 2).In addition, 2 embryos out of 15 analyzed showed AVSDs (Supplemental Fig. 2K). Despite of the obvious myocardial phenotype, we could see no differences in the relative distribution of endocardial cells, myocardial cells and cardiac fibroblasts (Supplemental Fig. 3). The muscular VSDs and myocardial defects were recapitulated independently using the *Mox2Cre* driver line (Tallquist and Soriano, 2000), which shows a chimeric recombination pattern in the epiblast (Fig. 2J and K). Collectively, these findings suggest that the death of the epiblast-specific *Trim33* mutants results from cardiac failure.

Histological analysis of mesendoderm-specific *Trim33:TCre* mutants at E13 revealed a subtle delay in formation of the inter-ventricular septum (Table 4 and Supplemental Fig. 4), while cardiac progenitor-specific (*Trim33:Nkx2-5Cre*), endothelium-specific (*Trim33:Tie2Cre*) and neural crest-specific (*Trim33:Wnt1Cre*) mutants did not display any detectable external or histological phenotypes (Table 4). Interestingly, those *Trim33*^{FF}*:Sox2Cre* mutants that survived beyond E15 showed cleft palate (Fig. 2L, M). However, deletion of *Trim33* in cell types that critically contribute to palatogenesis, i.e., neural crest, endothelium and epithelium using *Wnt1Cre, Tie2Cre* or *K14Cre* drivers, respectively, did not result in palatal defects (Table 4) (Lane et al., 2015). Therefore, we examined whether the progressive cardiac failure would lead to hypoxia, which has been shown to result in a failure of palatogenesis (Jones et al., 2008). Indeed, *Trim33:Sox2Cre* mutants showed a notable increase in hypoxic regions in the mesenchyme of prefusion palatal shelves (Fig. 2N vs. O). In addition, we compared histological phenotypes of several endoderm-derivatives, e.g., esophagus, bronchi and lungs between controls and *Trim33:Sox2Cre* mutants; none of them showed detectable phenotype in mutants when compared to control littermates (Supplemental Fig. 5). These experiments suggested that Trim33 is required for normal embryogenesis during a narrow time window at late gastrulation or soon after it, and that epiblast-specific *Trim33* deficiency results in cardiac and secondary craniofacial defects and premature death. However, Trim33 does not appear to be important for development of mesodermal cell lineages after their initial specification.

It was previously reported that the epiblast-specific *Trim33* mutants die soon after gastrulation and show expansion of Nodal signaling in the node (Morsut et al., 2010). In contrast, our *Trim33*^{FF}*:Sox2Cre* mutants survive until E13–15, and show no phenotypes associated with inappropriate Nodal signaling (e.g. A-P or L-R patterning defects). To examine whether Smad-dependent Nodal/TGF-β signaling contributes to the observed *Trim33*^{FF}*:Sox2Cre* lethal phenotype, we generated epiblast-specific *Trim33* mutants, which were heterozygous for the Smad4 gene (*Trim33*^{FF}*:Smad4*^{FWT}*:Sox2Cre*), and compared their survival rate and cardiac phenotype to those of *Trim33*^{FF}*:Sox2Cre* mutant and Cre-negative control littermates. At E13, the survival rate of *Trim33* mutants was about 40% of the expected frequency, while the corresponding rate of *Trim33*^{FF}*:Smad*^{FWT}*:Sox2Cre* mutants

was more than 70% ((Fig. 2H) Chi-Sq $X^2(1) = 6$; $p > 0.05$). Concordant with the increased rate of survival, the compact myocardium was thicker in *Trim33*^{FF}*:Smad*^{FWT}*:Sox2Cre* mutants than in *Trim33*^{FF}*:Sox2Cre* mutants, albeit still thinner than in controls (Fig. 2G). However, the trabecular phenotype was not rescued by *Smad4* heterozygosity. Likewise, at E13.5 most of the Trim33 mutants that were heterozygous for *Smad4* displayed VSDs (Fig. 2G); no surviving *Trim33*^{FF}*:Smad*^{FWT}*:Sox2Cre* mutants could be found at E18 (Fig. 2I). These data show that the lethal cardiac phenotype of the present epiblast-specific *Trim33* mutants can be partially rescued by *Smad4* haploinsufficiency suggesting that one possible role of Trim33 is to attenuate Smad-dependent TGF-β superfamily signaling in mouse embryos during a narrow time window following mesoderm induction.

3.3. Trim33 is efficiently deleted already at the pre-streak stage in Trim33:Sox2Cre embryos

Since our results showing that *Trim33:Sox2Cre* mutants survived until E13 significantly differed from those of Morsut et al. (2010), we wondered whether this could be due to inability of Cre recombinase to induce effective recombination in our conditional allele. We first used whole-mount *in situ* hybridization and a specific probe, which recognizes sequences encoded by exons 2–4 (flanked by loxP sites in the floxed allele) of the *Trim33* gene, to show that the *Trim33* mRNA was efficiently recombined at E8.5 (Fig. 3A and B). Next, we harvested both mutant and control embryos at the pre-streak stage (TS9), mid-streak stage (TS10) and head-fold stage (TS11) and analyzed them using antibodies that specifically recognize Trim33 and T (Brachyury, mesendoderm marker) (Fig. 3C–H). This assay demonstrated that Trim33 protein was efficiently ablated already at the pre-streak stage before mesendoderm induction (Fig. 3C–D). In addition, we analyzed E8.5 embryos for *T* expression to see whether a similar expansion of the anterior node could be seen in our mutants as what was reported by Morsut et al. (2010). Concordant with the lack of early embryonic death soon after gastrulation, we could not detect any differences in *T* expression between controls and mutants (Fig. 3I–L). At the head-fold stage, we could not detect obvious differences in cardiac crescent-specific *Nkx2-5* staining (Fig. 3M, N). These results show that the *Trim33* gene is effectively recombined by *Sox2Cre* and that Trim33 protein was already ablated at the pre-streak stage, and thus confirm that Trim33 is not required for mesendoderm induction in mouse embryos *in vivo*.

3.4. Trim33 deficiency results in increased cardiogenic differentiation in vitro

To further examine the role of Trim33 in cardiac progenitor cell differentiation, we used an embryoid body (EB) culture assay and embryonic stem (ES) cells that were homozygous for the *floxed Trim33* gene (Kim and Kaartinen, 2008) and carried the ubiquitously expressed Cre recombinase estrogen receptor fusion gene (Ruzankina et al., 2007) (Fig. 4A). This cell system allows for controlled inactivation of *Trim33* in EB cultures by 4-OHT (4-hydroxytamoxifen) treatment at day 4 of differentiation, i.e., during later stages of mesoderm induction (Fig. 4B). Since our objective was to investigate the role of *Trim33* in developmental events mimicking *in vivo* embryogenesis as closely as possible (within the limits of the EB culture technique), ES cells were allowed to undergo spontaneous differentiation in a suspension culture on ultra-low attachment dishes (Xi et al., 2011). Cre-induction by 4-OHT administration resulted in gradual decrease on Trim33 protein levels,

and no Trim33 protein was detected after the second day of induction (Fig. 4O). In contrast, *Gsc* mRNA expression levels were comparable between 4-OHT-induced mutant (*Trim33*^{FF}*:UbcCre*^{ERT2}, 4-OH^{+}) and non-induced control (*Trim33*^{FF}*:UbcCre*^{ERT2}, 4-OHT^{-}) cultures (on days 5 and 7) demonstrating that this treatment regimen allowed equivalent initiation of mesoderm induction in both 4-OHT negative and -positive cultures (Fig. 4B). Morphologically, control and mutant EBs remained indistinguishable for three days after 4-OHT induction (Fig. 4C and D).

Next, we harvested both the *Trim33* mutant and control EBs at day 7 and subjected them to genome-wide RNA-Seq transcriptome analysis. Of the 523 differentially expressed *Trim33*-dependent genes ($p < 0.05$), 58 were down-regulated (fold change ≤0.66) and 16 were up-regulated (fold change ≥1.5) when adjusted for False Discovery Rate of 0.1 (Table 1 in Appendix 1; GEO Submission GSE80166). Gene Set Enrichment Assay (GSEA) showed that genes associated with contractile fibers, muscle development and heart contraction were among those showing highest upregulation in *Trim33* mutant EBs (Fig. 4E and Supplemental Table 1). Consistent with expression changes, the number of beating EBs was higher in 4-OHT-induced than in non-induced cultures between days 9 and 11 of differentiation (Fig. 4F). We also stained both control and mutant EBs for Trim33 and for sarcomeric myosin (anti-MF20 antibody). Mutant EBs were completely negative for the strong nuclear Trim33 staining seen in controls (Fig. 4G vs. H), while staining patterns of MF20 were variable both in control and mutant EBs; some EBs showed large MF20-positive clusters (Fig. 4G-left and Fig. 4H-left), others showed more scattered MF20-positive cells (Fig. 4G-right and Fig. 4H-right). Next, we quantified the number of cardiac progenitor cells in controls and mutants at day 6 of EB differentiation using FACS together with antibodies, which specifically recognize Cxcr4 and Flk1 antigens (Cai et al., 2013). This assay showed that the mutant EBs displayed about 40% reduction in a number of Cxcr4^{+}, Flk1^{+} -double positive cardiac progenitor cells when compared to control EBs (Fig. 4I–K). Gene sets associated with Foxa2 signaling, cytosolic ribosomes and peptide chain elongation were among those that were down-regulated in mutant EBs when compared to controls (Fig. 4L, and Supplemental Table 1). Collectively these data suggest that deletion of *Trim33* in EBs following mesoderm induction results in accelerated myocardial differentiation, while the size of the precardiac mesoderm progenitor cell population is reduced.

Next we compared protein levels of Mesp1, Eomes, Foxa2 and Smad4,i.e., transcription factors/co-regulators controlling definitive endoderm and precardiac mesoderm formation, between control and mutant samples during EB differentiation (Fig. 4O, P and Supplemental Fig. 6). Mesp1 and Smad4 did not show significant differences between control and mutant EBs. Foxa2 protein levels were consistently higher in mutant EBs at day 6 and lower at day 7 of differentiation, while Eomes levels in mutants were comparable to those of controls at days 4 and 5 of differentiation and lower at days 6 and 7 of differentiation. These findings suggest that dynamic expression of Eomes and Foxa2 proteins was modestly but consistently altered in mutant EBs during the course of EB differentiation (Fig. 4O, P), and that, in this context, Trim33 does not regulate Smad4 protein stability. A recent study showed that in addition to the endoderm, *Foxa2* is transiently expressed in cardiac progenitors that give rise to ventricular myocardium (Bardot et al., 2017). In both control and mutant embryos at E7.25–E7.50 (during gastrulation), *Foxa2* was expressed with comparable intensity in the

presumptive cardiogenic region of the primitive streak (Fig. 4M, N). In contrast, *Foxa2* expression in the mutant endoderm consistently appeared relatively weak when compared to that in control littermates (Fig. 4M, N).

3.5. Isl1-positive cardiac progenitors show reduced proliferation in Trim33:Sox2Cre mutants

To define the effect of *Trim33* deficiency on cardiac progenitor cell proliferation and survival, we stained the sections of E7.5–E8.0 embryos for Isl1 (cardiac progenitor cell and second heart field [SHF] marker) (Ma et al., 2008) and pHH3 (mitotic cell marker) or for Isl1 and cleaved caspase-3 (apoptotic cell marker). We detected no differences in the rate of apoptosis (data not shown), while Isl1-positive cardiac progenitors of *Trim33:Sox2Cre* mutants showed reduced cell proliferation when compared to those of age and stage-matched controls (Fig. 5A–L, O). Concordantly, SHF-derivatives (right ventricle and OFT) appeared smaller and shorter in stage-matched mutant embryos when compared to those of controls (Supplemental Fig. 7). We also used EdU incorporation assay to analyze cell proliferation in the Mef2-positive myocardial cells at E10. This analysis revealed no noticeable differences in cell proliferation between controls and *Trim33* mutants in the working myocardium (Fig. 5M–N, P). These results suggest that epiblast-specific *Trim33* deficiency results in transient reduction in cardiac progenitor cell proliferation during early cardiogenesis (at E7.5), while the rate of myocardial proliferation later during heart development (at E10) is indistinguishable between controls and mutants.

3.6. Trim33:cofactor complexes bind to many potential target genes in day 6 EBs

As shown above, Trim33 plays an irreplaceable role in mouse embryos *in vivo* and in mouse embryoid bodies *in vitro* during mesoderm induction. Trim33 has been shown to act as a chromatin reader (Xi et al., 2011), elongation factor (Bai et al., 2010), ubiquitin ligase (Dupont et al., 2009) and transcriptional coregulator (Vincent et al., 2012). While our present results provide partial evidence that, also in this context, a possible role of Trim33 could be to suppress TGF-β superfamily signaling, many questions, e.g., how TGF-β suppression is achieved and whether it has other unrelated roles in this context remains unknown. Trim33 lacks a DNA binding domain, and thus its interactions with DNA are thought to be mediated by nuclear co-factors. To gain a better understanding of mechanisms regulated by Trim33 during late gastrulation, and to identify sites that bind Trim33:cofactor complexes during late mesoderm induction, ChIP-Seq analysis using ChIP-validated anti-Trim33 antibodies (Isbel et al., 2015) was performed on chromatin prepared from EBs at day 6 of differentiation (Fig. 6A and B; GEO submission GSE 119874). This assay indicated that there was a total of 4426 binding events; 23% of them were located on promoter regions, 40% were intragenic and 37% were intergenic (Fig. 6C). Gene ontology analysis using *GREAT* (McLean et al., 2010) indicated that Trim33 was strongly enriched close to the genes implicated in stem cell maintenance (132 regions, 53 genes) and mesoderm development (80 regions, 39 genes) (Fig. 6D and Supplemental Table 2). List of genes associated with stem cell maintenance included *Fzd7, Sall4, Cbfa2t2, Sox2, Lin28a, Prdm14* and *Klf4*, and those associated with mesoderm morphogenesis included *Eomes, Fgf8, Nodal, Smad2/3, Six2, Pax2* and *Hnf1a* (for a complete list of genes, see Supplemental Tables 3A and 3B). However, binding to gene regions associated with mesendoderm induction, e.g., *T*

and *MixL1* (Xi et al., 2011) was not observed. One of the highest-ranking developmental disease ontology GO terms was VSD (17 gene regions); associated genes were *Tbx5, Nkx2-5, Pitx2, Rtn4* and *Vegfa*. To examine whether Trim33 peak regions were enriched in specific binding motifs, Homer motif analysis (Heinz et al., 2010) was performed. This assay revealed that the consensus motifs for Ctcf, Tead and Isl1 were enriched (31.8%, 16.6% and 12.8%, respectively) in the Trim33 peak sequences (Fig. 6E). Next, ChIP-Seq analyses using specific ChIP-validated Ctcf and H3K27ac antibodies were used to examine whether Trim33 binding regions were enriched in Ctcf peaks and to examine the degree to which Trim33 binding took place in putative active enhancer regions. These assays confirmed that 47% of Trim33 peaks overlapped with Ctcf binding sites; about 40% of the Trim33 and Ctcf occupied sites were enriched for H3K27 acetylation suggesting that these sites were active enhancers (Fig. 6F). Fig. 6G shows examples of Trim33 peaks, which were shared with H3K27ac but not with Ctcf (upstream of *Cbfa2t2*, a co-repressor of stem cell differentiation (Tu et al., 2016)), which were shared with Ctcf but not with H3K27ac (upstream of *Foxc2* and *Phc2* intragenic, regulators of mesoderm specification) and which were shared both with Ctcf and H3K27ac (*Runx1* intragenic, regulator of hematopoiesis). Importantly, Trim33 mutant cells showed a clear reduction of Trim33 occupancy in a number of target genes (Fig. 6H). Co-transfection of EB cells (day 4 of differentiation) with *Trim33* and *Ctcf* cDNAs and subsequent immunoprecipitation (day 6 of differentiation) demonstrated that Ctcf interacted, either directly or indirectly, with Trim33 (Fig. 6I). Next, we analyzed the functional association between Trim33 and Ctcf using a Bayesian network-based multiple instance learning algorithm (Panwar et al., 2016). This approach predicts gene-level functional associations through integrating RNA-Seq, protein docking, protein domain and pseudo amino acid compositions from available data sources. It yielded a probability score of 0.8021 for Trim33 and Ctcf indicating a high probability for functional association between these two genes. Since H3K27ac marks are known epigenetic signatures of enhancers (Creyghton et al., 2010) and Ctcf is known to be enriched in enhancer elements (DeMare et al., 2013; Song et al., 2011) and function in regulation of the cardiac epigenome (Monte et al., 2016; Rosa-Garrido et al., 2017), we explored the possibility of overlap between Trim33, Ctcf and H3K27ac peaks from our Chip-Seq data with that of published heart enhancer datasets. Interestingly, 38 genomic regions showing co-occupancy of Trim33 with either Ctcf or H3K27ac coincide with reproducible enhancer activity in the heart among tested enhancer elements reported in the VISTA Enhancer Browser (Visel et al., 2007) (Supplemental Table 4 and Supplemental Fig. 8).

Together, these data imply that in EBs during late mesoderm differentiation Trim33 participates in regulatory complexes that control many different molecular and cellular functions including stem cell maintenance and mesoderm differentiation, and that many of these complexes include the chromatin architectural and insulator protein Ctcf.

4. Discussion

In this study, we used tissue-specific knockout mouse models and ES cell-based *in vitro* differentiation assays to investigate the role of *Trim33* in mouse development. We found that epiblast-specific *Trim33* mutants display a spectrum of cardiac defects including poorly formed trabeculae, thin myocardium and VSDs, and die during late gestation. Muscular

VSDs have been thought to result from inadequate coalescence of trabeculae (Anderson et al., 2014; Captur et al., 2016), and thus it is likely that VSDs in *Trim33* mutants are secondary to trabecular defects. Deletion of *Trim33* in EBs results in functional and molecular changes that are consistent with increased myocardial differentiation with concomitant reduction of the cardiac progenitor pool. This *in vitro* finding is concordant with reduced proliferation of Isl1-positive cardiac progenitor cells *in vivo*. In addition, mutant embryos displayed shorter OFT at E10.0–11.5 and AVSDs (with incomplete penetrance) at E13.5; both phenotypes attributed to defects in the SHF (Black, 2007; Briggs et al., 2013). While a partial rescue of the *Trim33:Sox2Cre* phenotype by *Smad4* heterozygosity imply that one potential role of Trim33 is to regulate canonical TGF-β superfamily signaling, our ChIP-Seq assays reveal more than 4400 binding sites suggesting a large number of potential target genes and proteins.

The role of Trim33 in Nodal-induced mesoderm induction is controversial. Morsut et al. showed that Trim33 provides negative control to Nodal-induced Smad-mediated signaling processes both in extraembryonic and embryonic tissues (Morsut et al., 2010), while in a more recent study, Xi et al. suggested that proposed chromatin reader activity of Trim33:Smad2 complexes is required for Smad4:Smad2 complexes to gain access to Nodal response elements during mesoderm induction (Xi et al., 2011). Furthermore, Xi et al. discussed that the discrepancy between their results and those of Morsut et al. could be explained by the involvement of Trim33 in regulation of a negative feedback factor Lefty by Nodal. This explanation ignored the finding of Morsut et al., who showed that most of the epiblast-specific Trim33 mutants form mesoderm. However, in that study, the recombination efficiency and protein ablation dynamics were not addressed, and a possibility that the observed phenotypes could have been influenced by factors, such as incomplete recombination or extraordinary protein stability, was not excluded. Our current study clarifies this controversy: *Sox2Cre* induces the complete removal of the Trim33 protein already in the pre-streak stage embryos, and thus our results unambiguously demonstrate that the ability of the epiblast-specific mutant embryos to form the primitive streak and induce mesoderm is similar to that of controls.

The phenotypes of epiblast-specific *Trim33* mutants we describe here and those of germline mutants we and others have described earlier (Isbel et al., 2015; Kim and Kaartinen, 2008) differ from the phenotypes described by Morsut et al. (2010). While we cannot definitively explain the reasons behind these differences, it should be noted that the mice used in our studies are in the mixed genetic background, while those descripted by Morsut et al. were reported to be in the inbred C57BL6 background, although the substrain was not specified. Therefore, it is possible that the genetic background modifies the outcome of *Trim33* deletion.

Previous studies have shown that TGF-β superfamily signaling plays a multifaceted role during early cardiogenesis (Cai et al., 2012; de Pater et al., 2012). Activin signaling has been shown to repress cardiac differentiation and promote endoderm differentiation (Cai et al., 2012), while *Id* genes, the *bona fide* targets of BMPs, have been shown to be able to override pro-endoderm cues and promote the cardiogenic mesoderm differentiation program (Cunningham et al., 2017). Hence, it seems that a delicate balance between BMP and

Activin driven signaling processes controls progenitor cell allocation to cardiac mesoderm and definitive endoderm. Our current results suggest that at day 7 of EB differentiation, the pro-endoderm program is attenuated (both Eomes and Foxa2 protein levels, and Foxa2 pathway are reduced in *Trim33* mutant EBs) and the pro-cardiogenic program is promoted (the GSEA and EB contraction assays show enhanced cardiac differentiation). These findings, together with reduced cardiac progenitor cell proliferation in *Trim33* mutant embryos and reduced number of cardiac progenitors in EBs, are consistent with a model suggesting that Trim33 regulates a balance between pro-endoderm and pro-cardiogenic mesoderm signals, and that its loss results in premature cardiac progenitor cell differentiation and reduced cardiac progenitor cell proliferation, ultimately resulting in myocardial and septal defects in epiblast-specific *Trim33* mutant embryos during late gestation.

While several studies have associated Trim33 to TGF-β superfamily signaling (Dupont et al., 2005; He et al., 2006; Morsut et al., 2010; Xi et al., 2011), it also has been shown to display functions that are not related to TGF-βs (Bai et al., 2010; Isbel et al., 2015; Kulkarni et al., 2013; Wang et al., 2015). Here we show that Smad4 haploinsufficiency improved the cardiac phenotype of epiblast-specific *Trim33* mutants; however, the improvement was partial and not fully penetrant. To gain deeper insights to mechanisms by which Trim33 mediates its function during early embryogenesis, we screened binding sites of Trim33 protein complexes in differentiating EBs using ChIP-Seq. This assay shows that nearly half of more than 4000 Trim33 peaks were occupied by Ctcf, a chromatin architectural protein and a highly conserved transcriptional regulator. Ctcf, which also mediates long-range interactions and functions as an insulator protein (Arzate-Mejia et al., 2018), has been shown to recruit RSmads to specific subset of binding sites (Van Bortle et al., 2015). While the roles of Ctcf in Trim33-regulated processes during early embryogenesis are currently unknown, it is of interest to note that a similar enrichment of Trim33 at Ctcf and at CtcfL (Ctcf paralog) (Boris) binding sites in male mouse germ cells has recently been reported (Rivero-Hinojosa et al., 2017). Trim33 interaction with Ctcf has also been described in hematopoietic stem cells, in which Trim33 has been shown to function as an elongation factor regulating erythropoiesis (Bai et al., 2010). In this context, Trim33 and another elongation factor Cdk9, together with Pol-II and erythroid transcription factors, were shown to bind to upstream enhancers on the *Myb* gene, and loop to the Ctcf-binding site in *Myb* intron 1 (Stadhouders et al., 2012) to regulate *Myb* transcription. Ctcf has been shown to mediate genetic interactions underlying heart morphology and function (Gomez-Velazquez et al., 2017), and cardiac-specific deletion of *Ctcf* induces cardiac failure in mice (Rosa-Garrido et al., 2017). Concurrently, several genomic regions showing co-occupancy of Trim33 with either Ctcf or H3K27ac in our Chip-Seq data coincide with reproducible enhancer activity in the heart among tested enhancer elements reported in the VISTA Enhancer Browser. Given that the expression domains of enhancer elements in the VISTA database are primarily reported for E11.5 stages and are not stage-matched for our *in vivo* or EB data, we do not imply direct functional relevance to our study; the coincidental overlap is open to more detailed assessment from researchers studying gene-regulatory elements.

In summary, our study reveals that mouse embryos deficient in *Trim33* develop cardiac defects and cleft palate, which belong to the most common congenital birth defects in

humans. We show that Trim33 is required for appropriate development of precardiogenic mesoderm in a very narrow time window during late gastrulation. Thus, the epiblast-specific Trim33 mutant embryos provide an example of a situation in which common congenital birth defects are caused by an inappropriate regulation of early signaling processes preceding the organ formation itself, such as cardiogenesis or palatogenesis.

Supplementary Material

Refer to Web version on PubMed Central for supplementary material.

Acknowledgements

This study was supported in part by the NIH RO1 grants HL074862 and DE013085 (VK).

References

Agricola E, Randall RA, Gaarenstroom T, Dupont S, Hill CS, 2011 Recruitment of TIF1gamma to chromatin via its PHD finger-bromodomain activates its ubiquitin ligase and transcriptional repressor activities. Mol. Cell 43, 85–96. [PubMed: 21726812]

Anderson RH, Spicer DE, Brown NA, Mohun TJ, 2014 The development of septation in the four-chambered heart. Anat. Rec. (Hoboken) 297, 1414–1429. [PubMed: 24863187]

Andl T, Ahn K, Kairo A, Chu EY, Wine-Lee L, Reddy ST, Croft NJ, Cebra-Thomas JA, Metzger D, Chambon P, Lyons KM, Mishina Y, Seykora JT, Crenshaw EB 3rd, Millar SE, 2004 Epithelial Bmpr1a regulates differentiation and proliferation in postnatal hair follicles and is essential for tooth development. Development 131, 2257–2268. [PubMed: 15102710]

Arzate-Mejia RG, Recillas-Targa F, Corces VG, 2018 Developing in 3D: the role of CTCF in cell differentiation. Development 145.

Aucagne R, Droin N, Paggetti J, Lagrange B, Largeot A, Hammann A, Bataille A, Martin L, Yan KP, Fenaux P, Losson R, Solary E, Bastie JN, Delva L, 2011 Transcription intermediary factor 1gamma is a tumor suppressor in mouse and human chronic myelomonocytic leukemia. J. Clin. Investig 121, 2361–2370. [PubMed: 21537084]

Bai X, Kim J, Yang Z, Jurynec MJ, Akie TE, Lee J, LeBlanc J, Sessa A, Jiang H, DiBiase A, Zhou Y, Grunwald DJ, Lin S, Cantor AB, Orkin SH, Zon LI, 2010 TIF1gamma controls erythroid cell fate by regulating transcription elongation. Cell 142, 133–143. [PubMed: 20603019]

Bai X, Trowbridge JJ, Riley E, Lee JA, DiBiase A, Kaartinen VM, Orkin SH, Zon LI, 2013 TiF1-gamma plays an essential role in murine hematopoiesis and regulates transcriptional elongation of erythroid genes. Dev. Biol 373, 422–430. [PubMed: 23159334]

Bardot E, Calderon D, Santoriello F, Han S, Cheung K, Jadhav B, Burtscher I, Artap S, Jain R, Epstein J, Lickert H, Gouon-Evans V, Sharp AJ, Dubois NC, 2017 Foxa2 identifies a cardiac progenitor population with ventricular differentiation potential. Nat. Commun 8, 14428. [PubMed: 28195173]

Black BL, 2007 Transcriptional pathways in second heart field development. Semin.Cell Dev. Biol 18, 67–76. [PubMed: 17276708]

Briggs LE, Phelps AL, Brown E, Kakarla J, Anderson RH, van den Hoff MJ, Wessels A, 2013 Expression of the BMP receptor Alk3 in the second heart field is essential for development of the dorsal mesenchymal protrusion and atrioventricular septation. Circ. Res 112, 1420–1432. [PubMed: 23584254]

Cai W, Albini S, Wei K, Willems E, Guzzo RM, Tsuda M, Giordani L, Spiering S, Kurian L, Yeo GW, Puri PL, Mercola M, 2013 Coordinate Nodal and BMP inhibition directs Baf60c-dependent cardiomyocyte commitment. Genes Dev. 27, 2332–2344. [PubMed: 24186978]

Cai W, Guzzo RM, Wei K, Willems E, Davidovics H, Mercola M, 2012 A Nodal-to-TGFbeta cascade exerts biphasic control over cardiopoiesis. Circ. Res 111, 876–881. [PubMed: 22872153]

Captur G, Wilson R, Bennett MF, Luxan G, Nasis A, de la Pompa JL, Moon JC, Mohun TJ, 2016 Morphogenesis of myocardial trabeculae in the mouse embryo.J. Anat 229, 314–325. [PubMed: 27020702]

Creyghton MP, Cheng AW, Welstead GG, Kooistra T, Carey BW, Steine EJ, Hanna J, Lodato MA, Frampton GM, Sharp PA, Boyer LA, Young RA, Jaenisch R, 2010 Histone H3K27ac separates active from poised enhancers and predicts developmental state. Proc. Natl. Acad. Sci. U. S. A 107, 21931–21936. [PubMed: 21106759]

Cunningham TJ, Yu MS, McKeithan WL, Spiering S, Carrette F, Huang CT, Bushway PJ, Tierney M, Albini S, Giacca M, Mano M, Puri PL, Sacco A, Ruiz-Lozano P, Riou JF, Umbhauer M, Duester G, Mercola M, Colas AR, 2017 Id genes are essential for early heart formation. Genes Dev. 31, 1325–1338. [PubMed: 28794185]

Danielian PS, Muccino D, Rowitch DH, Michael SK, McMahon AP, 1998 Modification of gene activity in mouse embryos in utero by a tamoxifen-inducible form of Cre recombinase. Curr. Biol 8, 1323–1326. [PubMed: 9843687]

de Pater E, Ciampricotti M, Priller F, Veerkamp J, Strate I, Smith K, Lagendijk AK, Schilling TF, Herzog W, Abdelilah-Seyfried S, Hammerschmidt M, Bakkers J, 2012 Bmp signaling exerts opposite effects on cardiac differentiation. Circ. Res 110, 578–587. [PubMed: 22247485]

DeMare LE, Leng J, Cotney J, Reilly SK, Yin J, Sarro R, Noonan JP, 2013 The genomic landscape of cohesin-associated chromatin interactions. Genome Res. 23, 1224–1234. [PubMed: 23704192]

Dobin A, Davis CA, Schlesinger F, Drenkow J, Zaleski C, Jha S, Batut P, Chaisson M, Gingeras TR, 2013 STAR: ultrafast universal RNA-seq aligner. Bioinformatics 29, 15–21. [PubMed: 23104886]

Dupont S, Mamidi A, Cordenonsi M, Montagner M, Zacchigna L, Adorno M, Martello G, Stinchfield MJ, Soligo S, Morsut L, Inui M, Moro S, Modena N, Argenton F, Newfeld SJ, Piccolo S, 2009 FAM/USP9x, a deubiquitinating enzyme essential for TGFbeta signaling, controls Smad4 monoubiquitination. Cell 136, 123–135. [PubMed: 19135894]

Dupont S, Zacchigna L, Cordenonsi M, Soligo S, Adorno M, Rugge M, Piccolo S, 2005 Germ-layer specification and control of cell growth by Ectodermin, a Smad4 ubiquitin ligase. Cell 121, 87–99. [PubMed: 15820681]

Falk S, Joosten E, Kaartinen V, Sommer L, 2014 Smad4 and trim33/tif1gamma redundantly regulate neural stem cells in the developing cortex. Cerebr. Cortex 24, 2951–2963.

Gittenberger-de Groot AC, Calkoen EE, Poelmann RE, Bartelings MM, Jongbloed MR, 2014 Morphogenesis and molecular considerations on congenital cardiac septal defects. Ann. Med 46, 640–652. [PubMed: 25307363]

Gomez-Velazquez M, Badia-Careaga C, Lechuga-Vieco AV, Nieto-Arellano R, Tena JJ, Rollan I, Alvarez A, Torroja C, Caceres EF, Roy AR, Galjart N, Delgado-Olguin P, Sanchez-Cabo F, Enriquez JA, Gomez-Skarmeta JL, Manzanares M, 2017 CTCF counter-regulates cardiomyocyte development and maturation programs in the embryonic heart. PLoS Genet. 13, e1006985. [PubMed: 28846746]

Hayashi S, Lewis P, Pevny L, McMahon AP, 2002 Efficient gene modulation in mouse epiblast using a Sox2Cre transgenic mouse strain. Mech. Dev 119 (Suppl. 1), S97–S101. [PubMed: 14516668]

He W, Dorn DC, Erdjument-Bromage H, Tempst P, Moore MA, Massague J, 2006Hematopoiesis controlled by distinct TIF1gamma and Smad4 branches of the TGFbeta pathway. Cell 125, 929–941. [PubMed: 16751102]

Heinz S, Benner C, Spann N, Bertolino E, Lin YC, Laslo P, Cheng JX, Murre C, Singh H, Glass CK, 2010 Simple combinations of lineage-determining transcription factors prime cis-regulatory elements required for macrophage and B cell identities. Mol. Cell 38, 576–589. [PubMed: 20513432]

Hesling C, Lopez J, Fattet L, Gonzalo P, Treilleux I, Blanchard D, Losson R, Goffin V, Pigat N, Puisieux A, Mikaelian I, Gillet G, Rimokh R, 2013 Tif1gamma is essential for the terminal differentiation of mammary alveolar epithelial cells and for lactation through SMAD4 inhibition. Development 140, 167–175. [PubMed: 23154409]

Isbel L, Srivastava R, Oey H, Spurling A, Daxinger L, Puthalakath H, Whitelaw E, 2015 Trim33 binds and Silences a class of young endogenous retroviruses in the mouse testis; a novel component of

the arms race between retrotransposons and the host genome. PLoS Genet. 11, e1005693. [PubMed: 26624618]

Jones KL, Webster WS, Vaux KK, Benirschke K, 2008 Acardiac fetus: evidence in support of a vascular/hypoxia pathogenesis for isolated oral clefting. Birth Defects Res. A Clin. Mol. Teratol 82, 597–600. [PubMed: 18553490]

Kim J, Kaartinen V, 2008 Generation of mice with a conditional allele for Trim33. Genesis 46, 329–333. [PubMed: 18543301]

Kisanuki YY, Hammer RE, Miyazaki J, Williams SC, Richardson JA, Yanagisawa M, 2001 Tie2-Cre transgenic mice: a new model for endothelial celllineage analysis in vivo. Dev. Biol 230, 230–242. [PubMed: 11161575]

Koni PA, Joshi SK, Temann UA, Olson D, Burkly L, Flavell RA, 2001 Conditional vascular cell adhesion molecule 1 deletion in mice: impaired lymphocyte migration to bone marrow. J. Exp. Med 193, 741–754. [PubMed: 11257140]

Koulnis M, Pop R, Porpiglia E, Shearstone JR, Hidalgo D, Socolovsky M, 2011 8 5 Identification and analysis of mouse erythroid progenitors using the CD71/TER119 flow-cytometric assay. J. Vis. Exp 54.

Kulkarni A, Oza J, Yao M, Sohail H, Ginjala V, Tomas-Loba A, Horejsi Z, Tan AR, Boulton SJ, Ganesan S, 2013 Tripartite Motif-containing 33 (TRIM33) protein functions in the poly(ADP-ribose) polymerase (PARP)-dependent DNA damage response through interaction with Amplified in Liver Cancer 1 (ALC1) protein. J. Biol. Chem 288, 32357–32369. [PubMed: 23926104]

Lane J, Yumoto K, Azhar M, Ninomiya-Tsuji J, Inagaki M, Hu Y, Deng CX, Kim J, Mishina Y, Kaartinen V, 2015 Tak1, Smad4 and Trim33 redundantly mediate TGF-beta3 signaling during palate development. Dev. Biol 398, 231–241. [PubMed: 25523394]

Ma Q, Zhou B, Pu WT, 2008 Reassessment of Isl1 and Nkx2–5 cardiac fate maps using a Gata4-based reporter of Cre activity. Dev. Biol 323, 98–104. [PubMed: 18775691]

McLean CY, Bristor D, Hiller M, Clarke SL, Schaar BT, Lowe CB, Wenger AM, Bejerano G, 2010 GREAT improves functional interpretation of cis-regulatory regions. Nat. Biotechnol 28, 495–501. [PubMed: 20436461]

Minette MS, Sahn DJ, 2006 Ventricular septal defects. Circulation 114, 2190–2197. [PubMed: 17101870]

Monte E, Rosa-Garrido M, Karbassi E, Chen H, Lopez R, Rau CD, Wang J, Nelson SF, Wu Y, Stefani E, Lusis AJ, Wang Y, Kurdistani SK, Franklin S, Vondriska TM, 2016 Reciprocal regulation of the cardiac epigenome by chromatin structural proteins hmgb and Ctcf: IMPLICATIONS for transcriptional regulation. J. Biol. Chem 291, 15428–15446. [PubMed: 27226577]

Morsut L, Yan KP, Enzo E, Aragona M, Soligo SM, Wendling O, Mark M, Khetchoumian K, Bressan G, Chambon P, Dupont S, Losson R, Piccolo S, 2010 Negative control of Smad activity by ectodermin/Tif1gamma patterns the mammalian embryo. Development 137, 2571–2578. [PubMed: 20573697]

Moses KA, DeMayo F, Braun RM, Reecy JL, Schwartz RJ, 2001 Embryonic expression of an Nkx2–5/Cre gene using ROSA26 reporter mice. Genesis 31, 176–180. [PubMed: 11783008]

Niessen K, Karsan A, 2008 Notch signaling in cardiac development. Circ. Res 102, 1169–1181. [PubMed: 18497317]

Panwar B, Menon R, Eksi R, Li HD, Omenn GS, Guan Y, 2016 Genome-wide functional annotation of human protein-coding Splice variants using multiple instance learning. J. Proteome Res 15, 1747–1753. [PubMed: 27142340]

Papaioannou VE, Behringer RR, 2012 Early embryonic lethality in genetically engineered mice: diagnosis and phenotypic analysis. Vet. Pathol 49, 64–70. [PubMed: 21233329]

Perantoni AO, Timofeeva O, Naillat F, Richman C, Pajni-Underwood S, Wilson C, Vainio S, Dove LF, Lewandoski M, 2005 Inactivation of FGF8 in early mesoderm reveals an essential role in kidney development. Development 132, 3859–3871. [PubMed: 16049111]

Pieters T, Haenebalcke L, Hochepied T, D'Hont J, Haigh JJ, van Roy F, van Hengel J, 2012 Efficient and user-friendly pluripotin-based derivation of mouse embryonic stem cells. Stem Cell Rev. 8, 768–778. [PubMed: 22011883]

Poelmann RE, Jensen B, Bartelings MM, Richardson MK, Gittenberger-de Groot AC, 2016 The epicardium in ventricular septation during evolution and development In: Nakanishi T, Markwald RR, Baldwin HS, Keller BB, Srivastava D, Yamagishi H (Eds.), Etiology and Morphogenesis of Congenital Heart Disease: from Gene Function and Cellular Interaction to Morphology, Tokyo, pp. 115–123.

Pommier RM, Gout J, Vincent DF, Alcaraz LB, Chuvin N, Arfi V, Martel S, Kaniewski B, Devailly G, Fourel G, Bernard P, Moyret-Lalle C, Ansieau S, Puisieux A, Valcourt U, Sentis S, Bartholin L, 2015 TIF1gamma suppresses tumor progression by regulating mitotic checkpoints and chromosomal stability. Cancer Res. 75, 4335–4350. [PubMed: 26282171]

Quere R, Saint-Paul L, Carmignac V, Martin RZ, Chretien ML, Largeot A, Hammann A, Pais de Barros JP, Bastie JN, Delva L, 2014 Tif1gamma regulates the TGF-beta1 receptor and promotes physiological aging of hematopoietic stem cells. Proc. Natl. Acad. Sci. U. S. A 111, 10592–10597. [PubMed: 25002492]

Rajderkar S, Panaretos C, Kaartinen V, 2017 Trim33 regulates early maturation of mouse embryoid bodies in vitro. Biochem. Biophys. Rep 12, 185–192. [PubMed: 29090280]

Rao PS, Harris AD, 2018 Recent advances in managing septal defects: ventricular septal defects and atrioventricular septal defects. F1000Res 7.

Rivero-Hinojosa S, Kang S, Lobanenkov VV, Zentner GE, 2017 Testis-specific transcriptional regulators selectively occupy BORIS-bound CTCF target regions in mouse male germ cells. Sci. Rep 7, 41279. [PubMed: 28145452]

Rosa-Garrido M, Chapski DJ, Schmitt AD, Kimball TH, Karbassi E, Monte E, Balderas E, Pellegrini M, Shih TT, Soehalim E, Liem D, Ping P, Galjart NJ, Ren S, Wang Y, Ren B, Vondriska TM, 2017 High-resolution mapping of chromatin conformation in cardiac myocytes reveals structural remodeling of the epigenome in heart failure. Circulation 136, 1613–1625. [PubMed: 28802249]

Ruzankina Y, Pinzon-Guzman C, Asare A, Ong T, Pontano L, Cotsarelis G, Zediak VP, Velez M, Bhandoola A, Brown EJ, 2007 Deletion of the developmentally essential gene ATR in adult mice leads to age-related phenotypes and stem cell loss. Cell Stem Cell 1, 113–126. [PubMed: 18371340]

Sandell LL, Kurosaka H, Trainor PA, 2012 Whole mount nuclear fluorescent imaging: convenient documentation of embryo morphology. Genesis 50, 844–850. [PubMed: 22930523]

Sedmera D, Pexieder T, Vuillemin M, Thompson RP, Anderson RH, 2000 Developmental patterning of the myocardium. Anat. Rec 258, 319–337. [PubMed: 10737851]

Song L, Zhang Z, Grasfeder LL, Boyle AP, Giresi PG, Lee BK, Sheffield NC, Graf S, Huss M, Keefe D, Liu Z, London D, McDaniell RM, Shibata Y, Showers KA, Simon JM, Vales T, Wang T, Winter D, Zhang Z, Clarke ND, Birney E, Iyer VR, Crawford GE, Lieb JD, Furey TS, 2011 Open chromatin defined by DNaseI and FAIRE identifies regulatory elements that shape cell-type identity. Genome Res. 21, 1757–1767. [PubMed: 21750106]

Stadhouders R, Thongjuea S, Andrieu-Soler C, Palstra RJ, Bryne JC, van den Heuvel A, Stevens M, de Boer E, Kockx C, van der Sloot A, van den Hout M, van Ijcken W, Eick D, Lenhard B, Grosveld F, Soler E, 2012 Dynamic long-range chromatin interactions control Myb proto-oncogene transcription during erythroid development. EMBO J. 31, 986–999. [PubMed: 22157820]

Tallquist MD, Soriano P, 2000 Epiblast-restricted Cre expression in MORE mice: a tool to distinguish embryonic vs. extra-embryonic gene function. Genesis 26, 113–115. [PubMed: 10686601]

Tanaka S, Jiang Y, Martinez GJ, Tanaka K, Yan X, Kurosaki T, Kaartinen V, Feng XH, Tian Q, Wang X, Dong C, 2018 Trim33 mediates the proinflammatory function of Th17 cells. J. Exp. Med 215, 1853–1868. [PubMed: 29930104]

Tu S, Narendra V, Yamaji M, Vidal SE, Rojas LA, Wang X, Kim SY, Garcia BA, Tuschl T, Stadtfeld M, Reinberg D, 2016 Co-repressor CBFA2T2 regulates pluripotency and germline development. Nature 534, 387–390. [PubMed: 27281218]

Van Bortle K, Peterson AJ, Takenaka N, O'Connor MB, Corces VG, 2015 CTCF-dependent co-localization of canonical Smad signaling factors at architectural protein binding sites in D. melanogaster. Cell Cycle 14, 2677–2687. [PubMed: 26125535]

Venturini L, You J, Stadler M, Galien R, Lallemand V, Koken MH, Mattei MG, Ganser A, Chambon P, Losson R, de TH, 1999 TIF1gamma, a novel member of the transcriptional intermediary factor 1 family. Oncogene 18, 1209–1217. [PubMed: 10022127]

Vincent DF, Gout J, Chuvin N, Arfi V, Pommier RM, Bertolino P, Jonckheere N, Ripoche D, Kaniewski B, Martel S, Langlois JB, Goddard-Leon S, Colombe A, Janier M, Van Seuningen I, Losson R, Valcourt U, Treilleux I, Dubus P, Bardeesy N, Bartholin L, 2012 Tif1gamma suppresses murine pancreatic tumoral transformation by a Smad4-independent pathway. Am. J. Pathol 180, 2214–2221. [PubMed: 22469842]

Visel A, Minovitsky S, Dubchak I, Pennacchio LA, 2007 VISTA Enhancer Browser–a database of tissue-specific human enhancers. Nucleic Acids Res. 35, D88–D92. [PubMed: 17130149]

Wang E, Kawaoka S, Roe JS, Shi J, Hohmann AF, Xu Y, Bhagwat AS, Suzuki Y, Kinney JB, Vakoc CR, 2015 The transcriptional cofactor TRIM33 prevents apoptosis in B lymphoblastic leukemia by deactivating a single enhancer. Elife 4, e06377. [PubMed: 25919951]

Xi Q, Wang Z, Zaromytidou AI, Zhang XH, Chow-Tsang LF, Liu JX, Kim H, Barlas A, Manova-Todorova K, Kaartinen V, Studer L, Mark W, Patel DJ, Massague J, 2011 A poised chromatin platform for TGF-beta access to master regulators. Cell 147, 1511–1524. [PubMed: 22196728]

Yang X, Li C, Herrera PL, Deng CX, 2002 Generation of Smad4/Dpc4 conditional knockout mice. Genesis 32, 80–81. [PubMed: 11857783]

Zhang Y, Liu T, Meyer CA, Eeckhoute J, Johnson DS, Bernstein BE, Nusbaum C, Myers RM, Brown M, Li W, Liu XS, 2008 Model-based analysis of ChIP-seq (MACS). Genome Biol. 9, R137. [PubMed: 18798982]

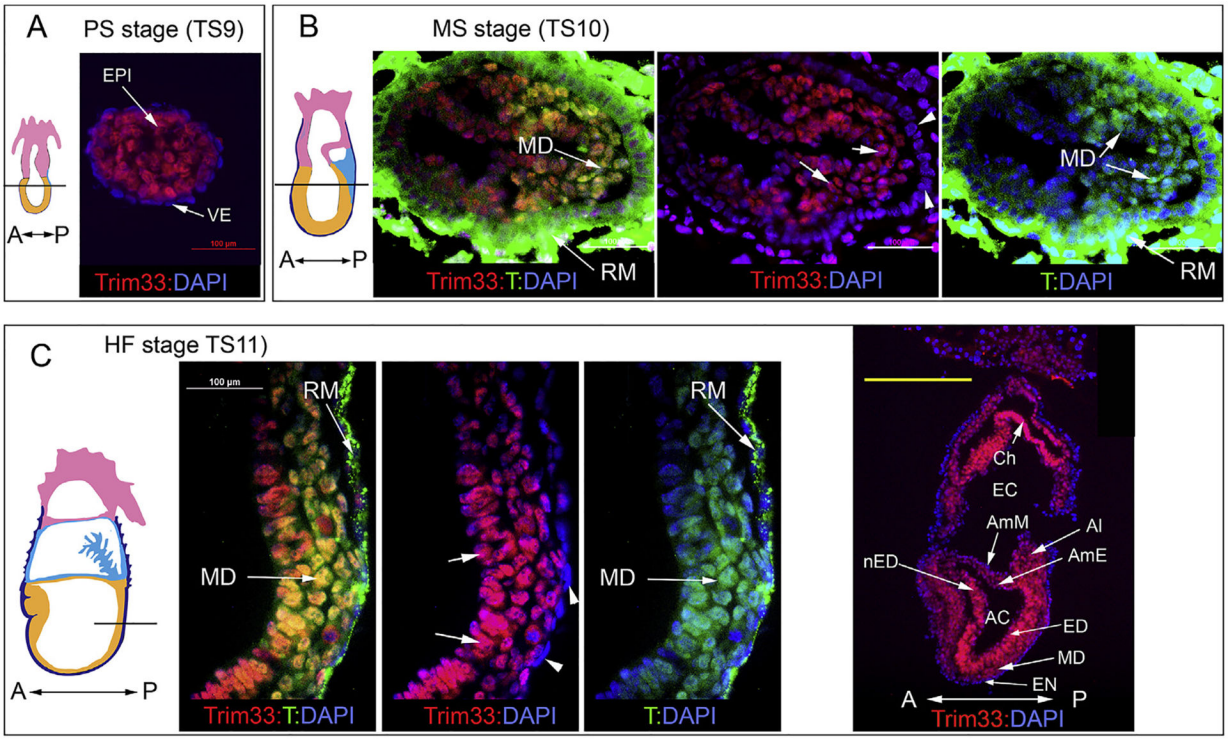

Fig. 1. Trim33 is expressed in mouse embryos before, during and after mesoderm induction.

A, pre-streak (PS) stage, B, mid-streak (MS) stage, C, head-fold (HF) stage embryos. Schematic drawings in A, B and C illustrate a lateral image of an embryo (re-drawn from 'www.emouseatlas.org'); horizontal line depicts the level of sections shown in A, B and C (left). Right hand image in C shows the lateral image of a HF-stage embryo (scale bars, 100 µm). EPI, epiblast; VE, visceral endoderm; MD, mesoderm; RM, Reichert's membrane; Ch, chorion; EC, exocoelomic cavity; AC, amniotic cavity; Al, allantois; AmM, amniotic mesoderm; AmE, Amniotic ectoderm; ED, ectoderm, nED, neural ectoderm; EN, endoderm; A, anterior; P, posterior. RM shows unspecific staining with T antibody (green).

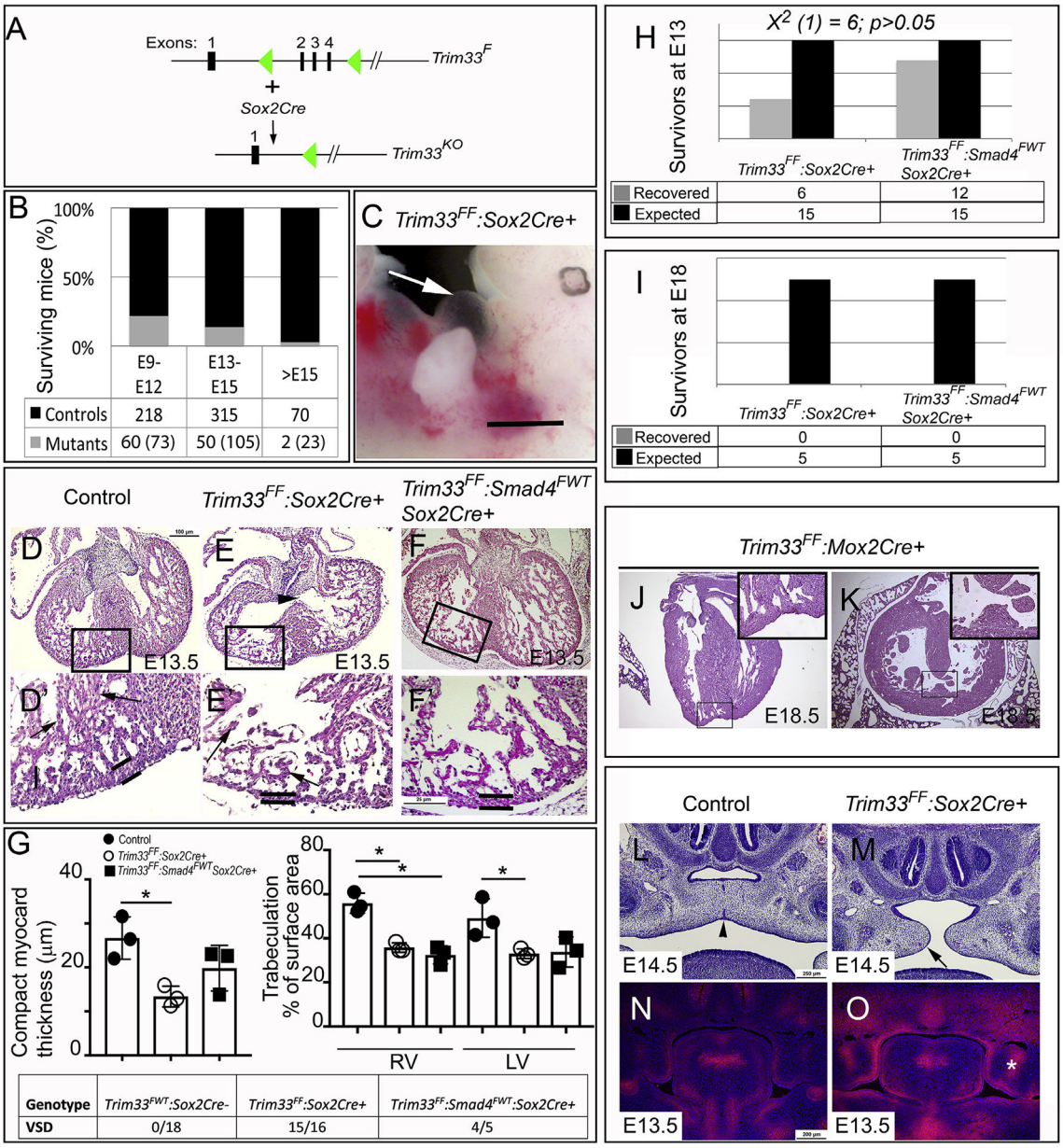

Fig. 2. Epiblast-specific deletion of *Trim33* results in embryonic death at E12-E15 *in vivo*.

A, schematic presentation of *Sox2Cre* induced recombination of the floxed Trim33 allele. B, epiblast-specific *Trim33* mutant embryos die between embryonic days 13 and 15 (expected numbers given in parentheses). C, *Trim33*^{FF}*:Sox2Cre* embryos often (10/31) display cardiac edema (C, white arrow). Scale bar, 1 mm. D-F, thin compact myocardium and VSD in *Trim33*^{FF}*:Sox2Cre*$^{+}$ mutants (E, E13.5), which can be partially rescued by *Smad4* heterozygosity (F). D, control; E, Trim33 mutant; F, *Trim33* mutant heterozygote for *Smad4* (scale bar, 100 µm). Boxed regions in D, E and F are shown as higher magnification in D', E' and F', respectively; 4-chamber view. Black arrows in D' and E' point to trabeculae, which are shorter and sparser in mutants (E'); black arrowhead in E points to the VSD (D–F, n = 5; scale bar, 25µm). G, left: quantification of compact myocardium thickness at E13.5 (n

= 3); black bar, controls; gray bar, *Trim33* mutants; white bar, *Trim33* mutants heterozygous for *Smad4*; error bars, sem. G, right: quantification of trabeculation (n = 3; for details –see Experimental Procedures); closed circles, controls; open circles, *Trim33* mutants; closed squares, *Trim33* mutants heterozygous for *Smad4*. G, bottom: summary of VSD frequency. H, the bar graph illustrates a genetic rescue of the $Trim33^{FF}$:$Sox2Cre^{+}$ lethal phenotype by *Smad4* heterozygosity. Black bars, recovered; gray bars, expected; X^2 (1) = 6; $p > 0.05$, i.e., the probability that there is no difference in the survival rate between $Trim33^{FF}$:$Sox2Cre^{+}$ and $Trim33^{FF}$:$Smad4^{FWT}$:$Sox2Cre^{+}$ embryos (at E13) is more than 5%. I, the bar graph shows that the $Trim33^{FF}$:$Sox2Cre^{+}$ mutants heterozygous for *Smad4* do not survive until E18. J–K, VSD in $Trim33^{FF}$:$Mox2Cre^{+}$ mutants at E18. Boxed areas shown as high-magnification images in insets (J-K, n = 3). L-M, $Trim33^{FF}$:$Sox2Cre^{+}$ mutants (E15) display cleft palate; frontal orientation-eye level; L, control; M, mutant. Black arrowhead in M points to the fusing midline seam; black arrow in N points to the cleft between palatal shelves (scale bar, 250 μm). N—O, increased hypoxia in $Trim33^{FF}$:$Sox2Cre^{+}$ mutants (E13); frontal orientation-eye level; N, control; O, mutant; Hypoxyprobe staining. White asterisk in O points to hypoxic regions in mutant palatal shelves (L-O, n = 3; scale bar, 250 μm).

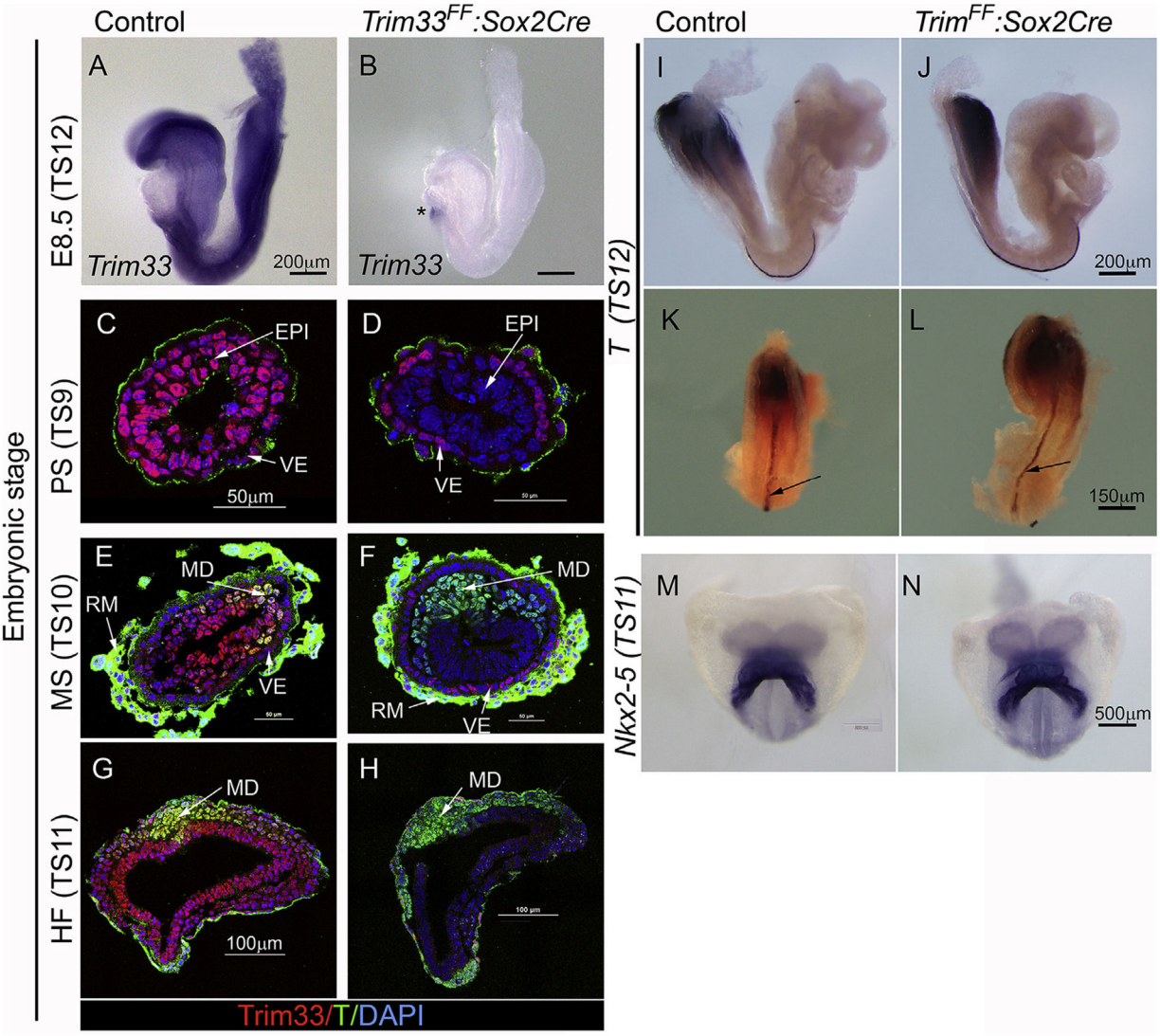

Fig. 3. *Sox2Cre*-induced recombination abrogates Trim33 in the prestreak-stage embryos.

A–B, whole mount *in situ* hybridization using a probe that recognizes sequences in exons 2–4 (flanked by loxP sites in the mutant); A, control; B, mutant (asterisk in B indicates a staining artifact) (n = 3; scale bars, 200 μm). C—H, immuno-staining for Trim33 and T in control (C, E, G) and *Trim33^{FF}:Sox2Cre* (D, F, H) sections prepared from embryos harvested at pre-streak stage (PS; C, D), mid-streak (MS; E, F) and head-fold (HS; G, H) stages. EPI, epiblast; VE, visceral endoderm; RM, Reichert's membrane (RM shows unspecific T-ab binding); MD, mesoderm (C—H, n = 5). RM shows unspecific staining with T antibody (green); scale bars: C—F, 50 μm; G–H, 100 μm). I-L, whole-mount in situ hybridization for *T* in control (I,K) and *Trim33^{FF}:Sox2Cre* mutant (J, L) embryos at E8.0; I–J, lateral images; K–L, dorsal-caudal images; black arrows (K, L) point to the positive signal in the notochord; scale bars: 200 μm in I–J; 150 μm in K–L (n = 3). M–N, Whole-mount *in situ* hybridization for *Nkx2-5* at HF-stage; frontal images (n = 5); scale bars, 500 μm.

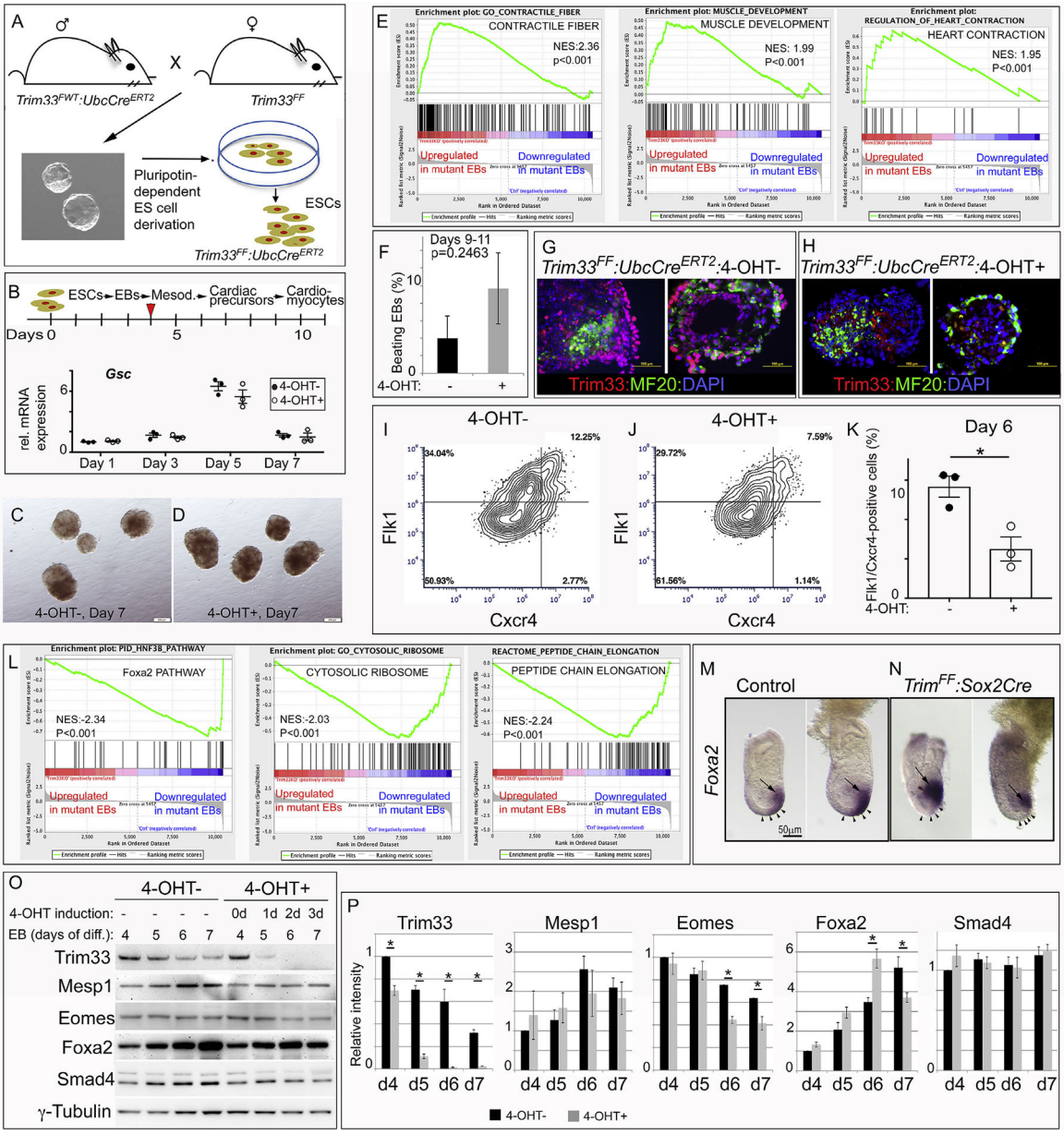

Fig. 4. Loss of Trim33 after mesoderm induction impairs normal embryoid body differentiation *in vitro*.

A, a schematic presentation outlining the establishment of ESC cultures. B, qRT-PCR analysis of *Gcs* expression in EBs (n = 3). Closed circles, 4-OHT-(controls); open circles, 4-OHT+ (*Trim33* mutants); induced with 4-OHT at day 4 (red triangle); horizontal lines, mean; vertical lines, sem. C–D, control and mutant EBs (4-OHT induction at day 4) on day 7 of differentiation. Scale bars, 200 µm. E, examples of GSEA indicated gene sets that were up-regulated in mutant EBs at day 7.0 (4-OHT induction at day 4; NES, normalized enrichment score). F, quantification of beating clusters in EBs at days 9–11 of differentiation; black bars, controls; gray bars, mutants; error bars, sem (n = 3; more than 100 EBs were counted in each set; p = 0.2463). G–H, control (G) and mutant EBs (day 7 of differentiation; 4-OHT induction at day 4) stained for Trim33 (red) and the sarcomeric

marker MF20 (green); counter staining with DAPI (blue) (n = 5) (please note that non-nuclear red fluorescence in G and H is released by dead cells; scale bars, 100 μm). I–J, FACS analysis of Flk1+ and Cxcr4+ cardiac precursors at day 6 of differentiation; I, control EBs; J, *Trim33* mutant EBs (4-OHT induction at day 4). K, bar graph depicting a reduced number of Flk1+:Cxcr4+ cardiac progenitor cells in mutants (opes circles) compared to controls (closed circles); error bars, sem; n = 3; *, $p < 0.05$. L, examples of GSEA indicated gene sets that were down-regulated in mutants at day 7.0 (4-OHT induction at day 4; NES, normalized enrichment score). M–N, whole-mount *in situ* hybridization for Foxa2 in control (M) and *Trim33*^{FF}*:Sox2Cre* mutant (N) embryos at E7.0 (displayed 2 representative embryos per genotype). Black arrows point to the presumptive cardiogenic region; black arrowheads point to the definitive endoderm (scale bars, 50 μm). O—P, control and mutant EBs (4-OHT induction at day 4) were harvested on days 4, 5, 6 and 7 of differentiation and protein extracts were subjected to Western blot analysis. O, representative blots showing Trim33, Mesp1, Eomes, Foxa2 and Smad4; γ-tubulin was used as a normalizer. P, the bar graphs show relative protein quantification of Trim33, Mesp1, Eomes, Foxa2 and Smad4 in control (black columns) and mutant EBs (gray columns) corresponding to the image in O (normalized to γ-tubulin; error bars, sem; *, $p < 0.05$; n = 3 [see also Supplemental Fig. 6]).

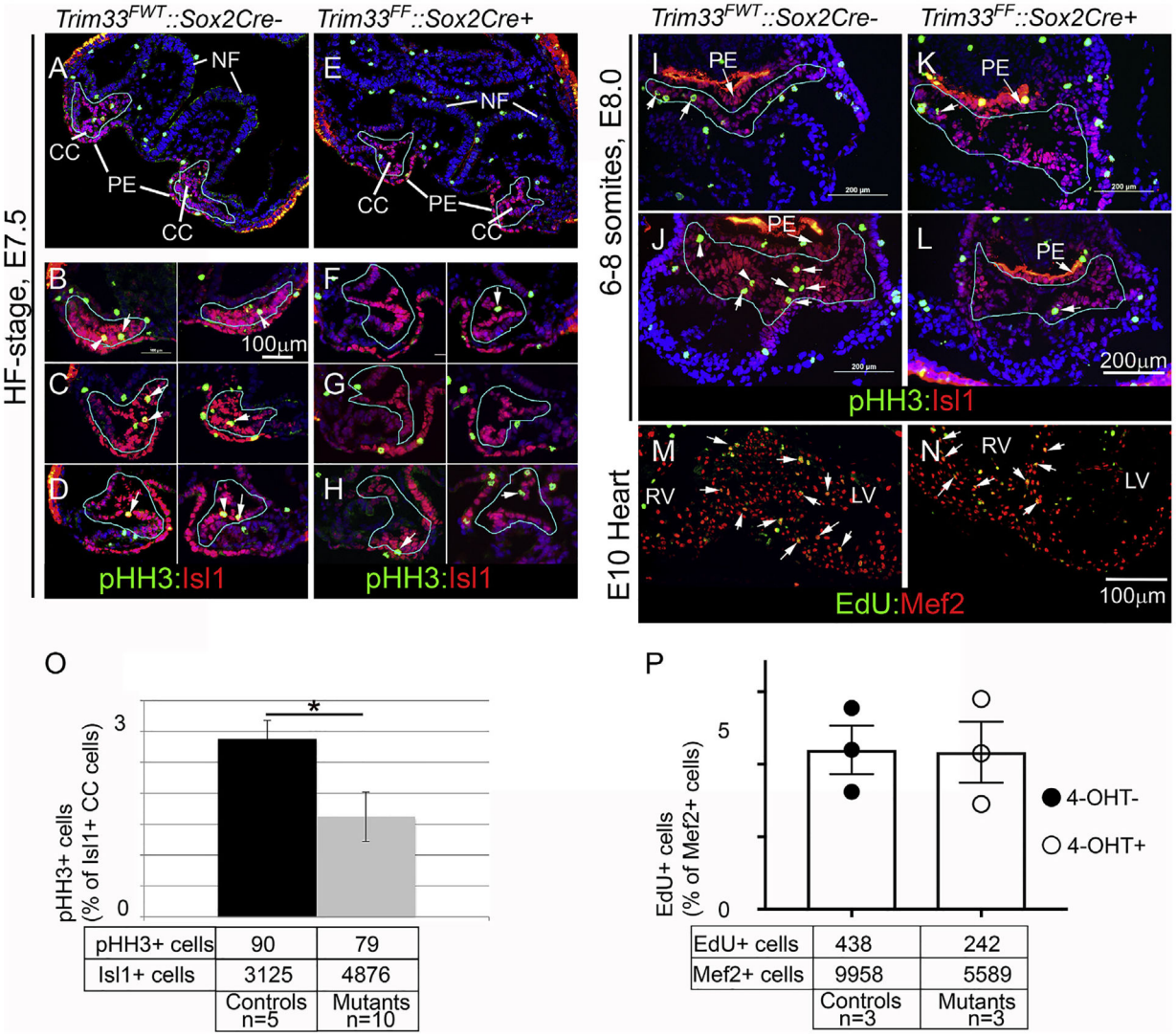

Fig. 5. *Trim33^{FF}:Sox2Cre* + mutants show reduced rate of cardiac progenitor cell proliferation at E7.5 and E8.0.

A–H, immunofluorescence microscopy of HF-stage embryos stained to detect pHH3 (mitotic marker; green) and Isl1 (cardiac progenitor marker; red). A–D controls, E–H *Trim33^{FF}:Sox2Cre* + mutants (A, E, low power images; B–D and F–H high power images; all different embryos; transverse orientation; counter staining with DAPI (blue). White arrows point to pHH3-positive cells. CC, cardiac crescent; PE, pharyngeal endoderm, NF, neural folds; scale bars for B–H (shown in B), 100 μm). I–L, immunofluorescence microscopy of 6–8 somite-stage embryos stained to detect pHH3 (mitotic marker; green) and Isl1 (cardiac progenitor marker; red). I–J, controls; K–L, *Trim33^{FF}:Sox2Cre*+ mutants; transverse orientation; counter staining with DAPI (blue). PE, pharyngeal endoderm; scale bars 200 μm. M–N, immunofluorescence microscopy of EdU-labeled E10.0 heart sections stained to detect EdU (green) and Mef2 (cardiomyocytes; red). White arrows point to EdU-positive cells. RV, right ventricle; LV, left ventricle; scale bars, 100 μm. O, quantification of mitotic cells in control and mutant embryos at E7.5–E8.0. Black bars, controls; gray bars,

mutants; error bars, sem; *, $p < 0.05$. P, quantification of EdU-positive cells in control and mutant embryos at E10. Closed circles, controls; open circles, mutants; error bars, sem.

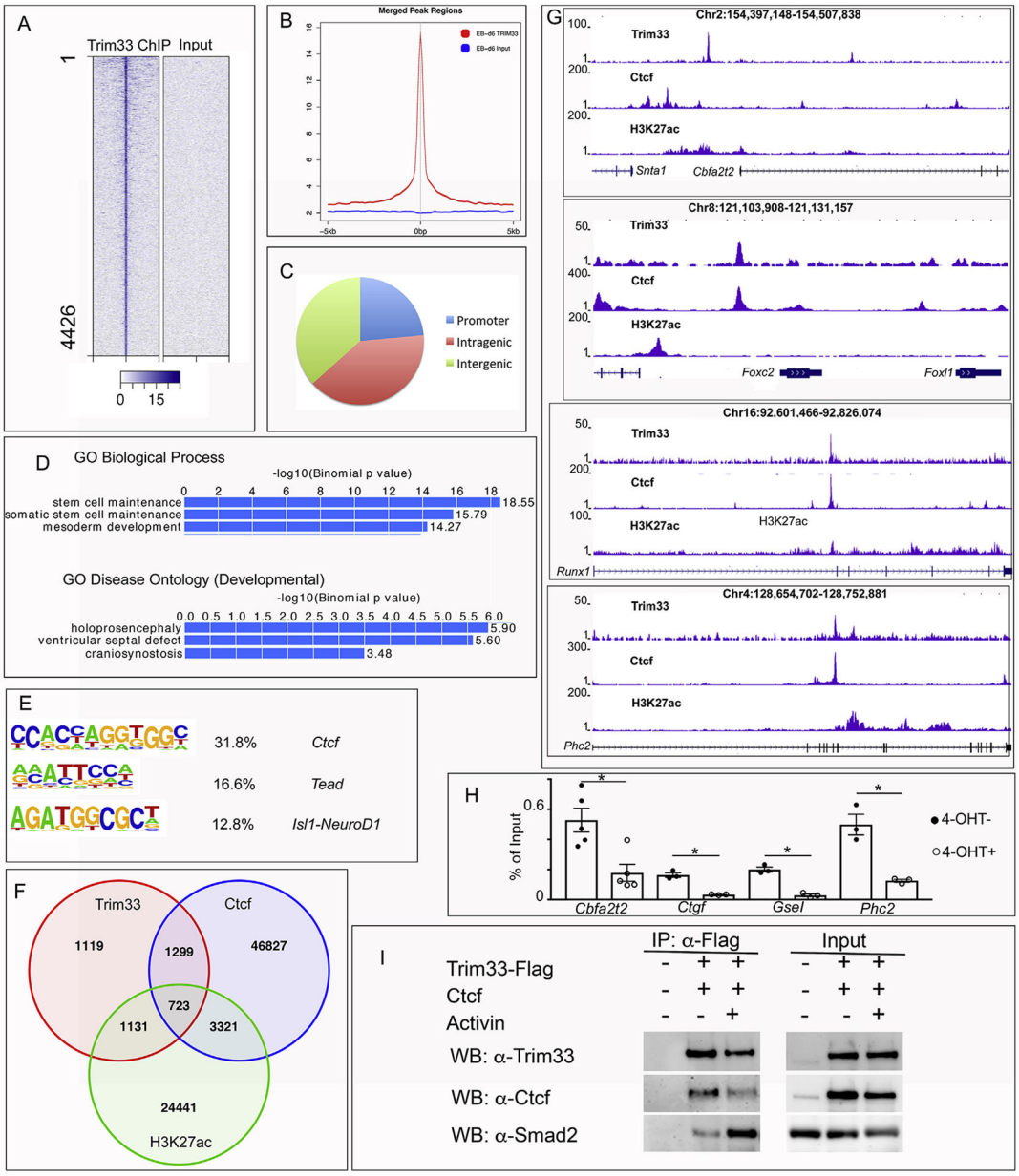

Fig. 6. Identification of *Trim33* target genes.

A, heat map showing Trim33 ChIP-Seq read density around the merged peak regions. B, signal intensity plot representing Trim33 and input ChIP-Seq profiles around the merged peak regions. C, pie chart displaying distributions of Trim33 peaks across promoter, intragenic and intergenic regions. D, functional annotation analysis using *GREAT* reveals that Trim33 preferentially binds to genes associated with stem cell maintenance and mesoderm formation (GO: Biological Process), and holoprosencephaly, VSD and craniosynostosis (GO: Disease Ontology (developmental diseases)). E, three most common consensus motifs recognized by Trim33 are Ctcf, Tead and Isl1 motifs. F, venn diagram showing the overlap of Trim33, Ctcf and H3K27ac target genes as identified by ChIP-Seq. G, examples of genome browser images depicting different Trim33, Ctcf and H3K27ac

profiles. H, ChIP-qPCR at enriched regions found near the four indicated genes; IP with the anti-Trim33 antibodies (controls, closed circles; mutants, open circles; n = 5 for *Cbfa2t2l*; n = 3 for *Ctgf, Gse1* and *Phc2*; *,$p < 0.05$). I, co-immunoprecipitation of Trim33 with Ctcf and Smad2 in EBs transfected with Flag-tagged *Trim33* cDNA and un-tagged *Ctcf* cDNAs with or without Activin stimulation (100 ng/ml, 40 min); n = 3.

Table 1

Antibodies used in the study.

Antigen	Use	Source	Cat.no
Trim33	IHC, WB	Sigma	HPA004345
Trim33	ChIP	Bethyl	A301–060A
T	IHC	R&D	AF2085
Mf20	IHC	DSHB	P3U-1
PHH3	IHC	Cell Signaling	9701
Isl1	IHC	DSHB	39.4d5
Mef2	IHC	Santa Cruz	Sc-313
Mesp1	WB	Thermo-Fisher	PA5–49441
Eomes	WB	Sigma	SAB2104422
Foxa2	WB	Novus	NBP2–02088
Flag	IP	Cell Signaling	8146
Smad4	WB	Cell Signaling	9515
Smad2	WB	Cell Signaling	5339
pSmad2	WB	Cell Signaling	8828
Ctcf	WB	Cell Signaling	3418
Ctcf	ChIP	Active Motif	61311
H3K27ac	ChIP	Active Motif	39133
Flk1	FACS	BD Pharmingen	560680
Cxcr4	FACS	BD Pharmingen	561734
Cd71	FACS	BD Pharmingen	553266
Ter119	FACS	BD Pharmingen	553673
Cd31	IHC	eBioscience	11–0311
Pdgfrα	IHC	Sigma	SAB4502140

Table 2

In situ hybridization probes used in the study.

Gene	Length	Position	Ref seq
Trim33	397	1155–1552[a]	NM_05310.3
Foxa2	1441	1–1441	BC160375.1
T	1755	1–1755	NM_001161832

[a]Corresponds to sequences of exons 2–4, which are deleted in mutant cells. The probe does not detect the mutant allele.

Table 3

Primers used in ChIP-qPCR assays.

Target	Primer Sequences	Product
Ctgf intragenic-S	5′cggctcccgggagcgtataa-3′	Chr10:24595457–24595597
Ctgf intragenic-AS	5′gctgggctggggctgct-3	(140bp)
Gsel intragenic-S	5′cacgcacctggctcccctg3′	Chr8:120528360–120528455
Gsel intragenic-AS	5′ggacctccaggcgctcttgc3′	(95 bp)
Cbfa2t2	5′cccggggagcttaaggtcatt3′	Chr2:154428142–154428294
5′upstream-S		(152bp)
Cbfa2t2	5′gctgctgcagctgggcc3′	
5′upstream -AS		
Phc2 intragenic -S	5′cccccattgtccagcagagg3′	Chr4:128511550–128711682
Phc2 intragenic -AS	5′cggcaaagcacggtatggaaaa3′	(132 bp)

Table 4

Summary of used Cre-lines and noticed phenotypes.

Driver	Affected tissue type	Developmental phenotype	Viability at birth
TCre(Perantoni et al., 2005)	mesendoderm	modest delay in ventricular septation	viable
Nkx2–5Cre(Moses et al., 2001)	cardiac mesoderm	none detected	viable
Wnt1Cre(Danielian et al., 1998)	neural crest, neural plate	none detected	viable
Tie2Cre(Kisanuki et al., 2001)	endothelium	none detected	viable
K14Cre(Andl et al., 2004)	epiderm	none detected	viable
Sox2Cre(Hayashi et al., 2002)	epiblast	VSD, thin myocardium, sparse trabeculae, cleft palate, death	not viable
Mox2Cre(Tallquist and Soriano, 2000)	epiblast	VSD	not viable